Albumin-STING Nanocomplex Reprograms HSPCs to Antitumor Neutrophils with Enhanced MHC I Antigen Presentation for Cancer Immunotherapy

Jinsong Tao[1, †], Hongyi Zhao[1, †], Chengyi Li[1], Hanning Wen[1], Fang Ke[1], Qiuxia Li[1], Miao He[1], Bo Wen[1], Zhongwei Liu[1], Wei Gao[1, 2, *], Duxin Sun[1, *]

[1] Department of Pharmaceutical Sciences, College of Pharmacy, Rogel Cancer Center, University of Michigan, Ann Arbor, MI 48109, USA

[2] Department of Pharmacology and Pharmaceutical Sciences, College of Pharmacy, University of Houston, TX, 77204, USA

[†] These authors contributed equally to this work

*Correspondence: wgao21@central.uh.edu (W.G.), duxins@umich.edu (D.S.)

Abstract

Recent evidence suggests that reprogramming hematopoietic stem and progenitor cells (HSPCs) into distinct neutrophil subsets could improve cancer immunotherapy. Although STING activation in dendritic cells and macrophages is well studied to enhance antitumor immunity, it is unknown whether and how STING activation can direct HSPCs toward antitumor neutrophils for cancer immunotherapy. Here, we developed an albumin-STING agonist nanocomplex (Nano ZSA-51D) that reprogramed HSPCs into $CD14^+ICAM\text{-}1^+$ neutrophils with enhanced MHC I antigen presentation. Nano ZSA-51D expanded HSPCs and skewed differentiation toward granulocyte-monocyte progenitors via STING-NF-κB-IL-6 signaling. It further reprogrammed immature ($CD101^-$) and mature ($CD101^+$) neutrophils into activated $CD14^+ICAM\text{-}1^+$ subsets through STING-NF-κB–TNF-α signaling. These neutrophils migrated from bone marrow to tumors for MHC I antigen presentation to activate tumor-specific $CD8^+$ T cell immunity. Adoptive transfer of immature/activated $CD14^+$ neutrophils combined with α-PD1 led to complete tumor regression of colon tumors. Nano ZSA-51D combined with α-PD1 achieved potent anticancer efficacy in colon and pancreatic cancer model with minimal toxicity. This study establishes Nano ZSA-51D as a novel strategy to reprogram HSPCs into antitumor neutrophils that mediate MHC I antigen presentation to activate CD 8^+ T cell tumor immunity.

One Sentence Summary: Albumin-STING agonist nanocomplex reprograms HSPCs into $CD14^+ICAM\text{-}1^+$ neutrophils that enhance MHC I-mediated tumor-specific CD 8^+ T cell immunity.

INTRODUCTION

Activation of the stimulator of interferon genes (STING) pathway plays a pivotal role in activating innate immunity to achieve anticancer efficacy.(*1*) Prior studies have primarily focused on STING activation to enhance antitumor immunity by stimulating dendritic cells (DCs) and macrophages to promote $CD8^+$ T cell responses.(*2-4*) In these myeloid cells, STING activation leads to either phosphorylation of interferon regulatory factor 3 (IRF3) to promote type I interferons (IFNs) release, or phosphorylation of nuclear factor κB (NF-κB) to produce proinflammatory cytokines (e.g., TNF-α, IL-6) for its anticancer immunity.(*5, 6*)

However, recent studies suggest that STING activation increases neutrophil infiltration into the tumor microenvironment (TME), correlating with improved efficacy of cancer immunotherapy.(*7-10*) Consistently, depletion of neutrophils diminishes the antitumor effects of STING agonists, suggesting that these neutrophils are critical contributors to the therapeutic response.(*7-9*) This clearly contrasts with earlier reports that high neutrophil infiltration in tumors, often categorized as polymorphonuclear myeloid-derived suppressor cells (PMN-MDSCs), was associated with immunosuppression and poor prognosis.(*11-16*) However, increasing evidence now supports that neutrophils can be reprogrammed into antitumor (N1) or protumor (N2) subsets.(*17-20*) The N1 neutrophils have antitumor properties by directly killing tumor cells or acting as antigen-presenting cells (APCs), potentially sensitizing tumors to anti-PD1 (α-PD1) therapy.(*21-27*) These findings suggest that STING agonists may reprogram neutrophils into distinct antitumor phenotypes rather than immunosuppressive PMN-MDSCs, which might offer a novel therapeutic opportunity. However, it is still unknown how STING agonists reprogram neutrophils toward an anti-tumor phenotype and the underlying antitumor mechanisms of neutrophils for cancer immunotherapy.

Furthermore, emerging evidence suggests that the development of antitumor (N1) or protumor (N2) neutrophils are likely to be determined early from hematopoietic stem and progenitor cells (HSPCs), rather than through interconversion within the TME.(*28-32*) For example, Garner et al. demonstrated that tumor-derived signals imprint immunosuppressive programming onto HSPCs, leading to the development of pro-tumor neutrophils.(*28, 29*) While Daman et al. showed that microbial immunotherapy could reprogram HSPCs to generate neutrophils resistant to pro-tumor conversion.(*30*) These findings highlight the therapeutic potential of directing neutrophil differentiation toward anti-tumor phenotypes at the progenitor stage, before exposure to tumor-

derived signals. Therefore, it is critical to know whether and how STING agonists can dictate the fate of neutrophil progenitors into anticancer subtypes of neutrophils by reprogramming HSPCs in bone marrow.

Here, we developed an albumin-STING agonist nanocomplex (Nano ZSA-51D) to reprogram HSPCs into anticancer $CD14^+ICAM\text{-}1^+$ neutrophils, which migrated from bone marrow to TME for MHC I antigen presentation to activate $CD8^+$ T cell antitumor immunity (**Fig. 1A**). The dimmer STING agonist ZSA-51D was synthesized from monomer STING agonist(*33*) and encapsulated into albumin nanoparticle. Nano ZSA-51D expanded HSPCs and skewed differentiation toward granulocyte-monocyte progenitors (GMPs) via STING-NF-κB-IL-6 signaling. It further reprogrammed the immature ($CD101^-$) and mature ($CD101^+$) bone marrow neutrophils into $CD14^+ICAM\text{-}1^+$ subsets through STING–NF-κB–TNF-α signaling, and thereby dramatically enhanced neutrophil migration from bone marrow to tumors. Interestingly, adoptive transfer of the immature $CD14^+$ neutrophils combined with α-PD1 therapy achieved complete regression of colon tumors. Furthermore, Nano ZSA-51D combined α-PD1 exhibited long-term anticancer efficacy with long-term immune memory in colon cancer model and potent therapeutic activity in pancreatic cancer model. Transcriptomic and immune profiling revealed that Nano ZSA-51D-induced $CD14^+$ neutrophils enhanced MHC I antigen presentation to activate tumor specific $CD8^+$ T cell immunity. This study provides a novel strategy using Nano ZSA-51D to reprogram HSPCs into anticancer neutrophils, which migrate from bone marrow to TME for MHC I antigen presentation to activate $CD8^+$ T cell antitumor immunity.

RESULTS

Albumin-STING Agonist Nanocomplex (Nano ZSA-51D) Potently Activated STING Pathway and Enhanced Neutrophil Infiltration into Tumors

Building on our previously developed monomeric STING agonist, ZSA-51,(*33*) we synthesized a novel non-CDN dimeric STING agonist, ZSA-51D, which exhibited superior STING pathway activation (**Fig. 1A, Left**). ZSA-51D is an ester-based prodrug, that requires hydrolysis by esterases to convert into its active acid form (ZSA-52D) before binding to STING protein. Both ZSA-51D and ZSA-52D were synthesized (**Fig. S1)**. Due to its enhanced cell permeability, ZSA-51D can be easily uptake inside cells and efficiently converted to ZSA-52D, resulting in potent and sustained STING activation. As anticipated, ZSA-51D showed no binding with human STING,

whereas ZSA-52D displayed a potent binding affinity to human STING, with an IC_{50} of 1.17 nM (**Fig. 1B**). In THP1-Blue™ ISG reporter cells, ZSA-51D demonstrated a superior EC_{50} of 5.1 nM, outperforming ZSA-52D (EC_{50} = 14.1 nM) and monomer ZSA-51 (EC_{50} = 52.6 nM) (**Fig. 1C**).

To facilitate systemically intravenous administration, we encapsulated ZSA-51D into an albumin nanocomplex (Nano ZSA-51D).(*34-36*) The average particle size of Nano ZSA-51D was 100.2 ± 4.3 nm (**Fig. 1D**). Notably, Nano ZSA-51D exhibited an 11.6-fold enhancement in STING activation (EC_{50} = 0.44 nM) compared to free ZSA-51D (EC_{50} = 5.1 nM) in THP1-Blue™ ISG cells (**Fig. 1E**). Western blot analysis further confirmed that Nano ZSA-51D significantly enhanced phosphorylation of STING and downstream effectors IRF3 and NF-κB p65 (**Fig. 1F),** thereby promoting the production of IFN-β, TNF-α and IL-6 (**Fig. 1G**). These results indicate that Nano ZSA-51D potently activates both the STING-IRF3 and STING-NF-κB pathway.

To further verify whether Nano ZSA-51D enhances neutrophil infiltration in tumors, we analyzed the neutrophil population in tumors, bone marrow and blood circulation in MC-38 tumor-bearing mice 24 hours after 3 doses administration (1 mg/kg, I.V.) using flow cytometry (**Fig. 1H**). In MC-38 tumors, Nano ZSA-51D dramatically increased tumor-infiltrating neutrophils from 11.2% to 56.7% of $CD45^+$ immune cells, a substantially greater enhancement than that observed with free ZSA-51D (**Fig. 1I**). Similar effects were observed in mice inoculated KPC 6620 pancreatic cancer cells, where Nano ZSA-51D significantly increased tumor-infiltrating neutrophils from 32.7% to 59.0% (**Fig. S2**). In the bone marrow, free ZSA-51D and Nano ZSA-51D increased proportion of neutrophils from 50.1% to 59.7% and 63.3% among $CD45^+$ cells, respectively (**Fig. 1J**). In blood circulation, Nano ZSA-51D also increased total circulating neutrophils, but which was much less than free ZSA-51D (**Fig. 1K**). Collectively, these findings demonstrate that Nano ZSA-51D significantly enhanced neutrophil expansion in vivo and neutrophil infiltration into tumors in both colon and pancreatic cancer models.

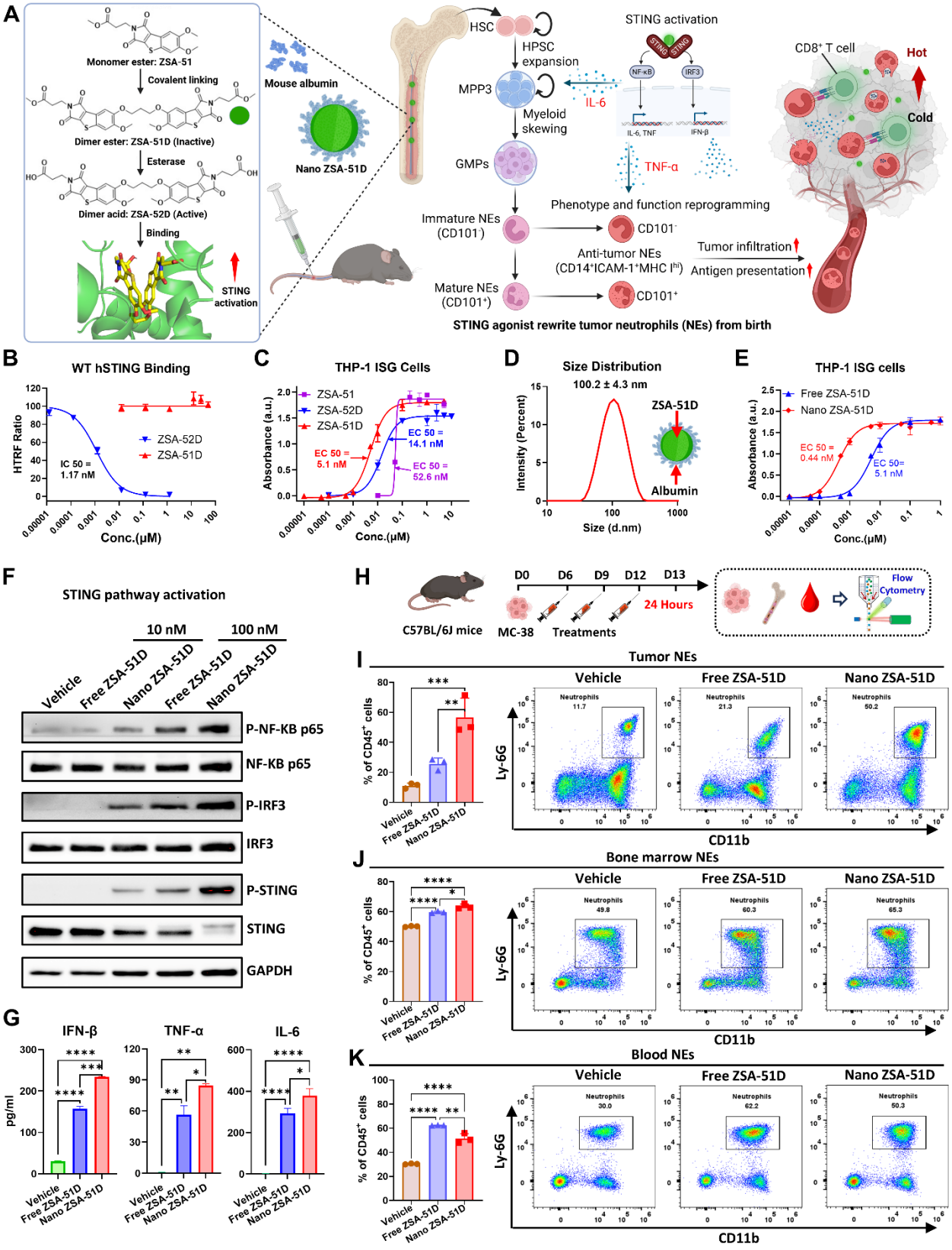
A
Monomer ester: ZSA-51
Covalent linking
Dimer ester: ZSA-51D (Inactive)
Esterase
Dimer acid: ZSA-52D (Active)
Binding
STING activation
Mouse albumin
Nano ZSA-51D
HSC
HPSC expansion
MPP3
Myeloid skewing
GMPs
Immature NEs (CD101⁻)
Mature NEs (CD101⁺)
STING activation
IL-6
TNF-α
Phenotype and function reprogramming
CD101⁻
CD101⁺
Anti-tumor NEs (CD14⁺ICAM-1⁺MHC I^hi)
Tumor infiltration
Antigen presentation
CD8⁺ T cell
Hot
Cold
STING agonist rewrite tumor neutrophils (NEs) from birth
B
WT hSTING Binding
HTRF Ratio
IC 50 = 1.17 nM
ZSA-52D
ZSA-51D
Conc.(μM)
C
THP-1 ISG Cells
Absorbance (a.u.)
ZSA-51
ZSA-52D
ZSA-51D
EC 50 = 5.1 nM
EC 50 = 14.1 nM
EC 50 = 52.6 nM
Conc.(μM)
D
Size Distribution
100.2 ± 4.3 nm
Intensity (Percent)
ZSA-51D
Albumin
Size (d.nm)
E
THP-1 ISG cells
Absorbance (a.u.)
Free ZSA-51D
Nano ZSA-51D
EC 50 = 0.44 nM
EC 50= 5.1 nM
Conc.(μM)
F
STING pathway activation
10 nM
100 nM
Vehicle
Free ZSA-51D
Nano ZSA-51D
Free ZSA-51D
Nano ZSA-51D
P-NF-KB p65
NF-KB p65
P-IRF3
IRF3
P-STING
STING
GAPDH
G
IFN-β
TNF-α
IL-6
pg/ml
Vehicle
Free ZSA-51D
Nano ZSA-51D
H
C57BL/6J mice
D0
D6
D9
D12
D13
24 Hours
MC-38
Treatments
Flow Cytometry
I
Tumor NEs
Vehicle
Free ZSA-51D
Nano ZSA-51D
% of CD45⁺ cells
Neutrophils 11.7
Neutrophils 21.3
Neutrophils 50.2
Ly-6G
CD11b
J
Bone marrow NEs
Vehicle
Free ZSA-51D
Nano ZSA-51D
% of CD45⁺ cells
Neutrophils 49.8
Neutrophils 60.3
Neutrophils 65.3
Ly-6G
CD11b
K
Blood NEs
Vehicle
Free ZSA-51D
Nano ZSA-51D
% of CD45⁺ cells
Neutrophils 30.0
Neutrophils 62.2
Neutrophils 50.3
Ly-6G
CD11b

1

Figure 1. Nano ZSA-51D potently stimulated STING pathway and enhanced neutrophil infiltration into tumor.

(A) Schematic illustration of Nano ZSA-51D that reprograms HSPCs into antitumor neutrophils for cancer immunotherapy. Dimeric STING agonist ZSA-51D derived from monomeric STING agonist ZSA-51 was encapsulated into mouse albumin to form Nano ZSA-51D. Chemical structures of ZSA-51, ZSA-51D and its acid form, ZSA-52D, along with molecular docking simulation showing ZSA-52D (yellow) binding to the STING protein (green, PDB: 6UKZ), performed using AutoDock. Nano ZSA-51D expands HSPCs and skews granulocyte–monocyte progenitor (GMP) differentiation via STING–NF-κB–IL-6 signaling. It reprograms immature ($CD101^{-}$) and mature ($CD101^{+}$) bone marrow neutrophils into $CD14^{+}ICAM\text{-}1^{+}$ subsets through STING–NF-κB–TNF-α signaling, promoting neutrophil migration to tumors and enhancing antigen presentation to potentiate antitumor $CD8^{+}$ T cell responses.

(B) Binding affinity of ZSA-51D and ZSA-52D to wild-type (WT) human STING (hSTING) protein, determined by Homogeneous Time-Resolved Fluorescence (HTRF) assay.

(C) STING pathway activation was assessed in THP1-Blue ISG reporter cells with virous concentrations of ZSA-51D and ZSA-52D for 24 hours, demonstrating induction of the STING–IRF signaling cascade.

(D) Particle size distribution and schematic structure of Nano ZSA-51D.

(E) Comparison of STING-IRF pathway activation by free and Nano ZSA-51D in THP1-Blue ISG reporter cells after 24-hour treatment.

(F) Western blot analysis of the activation of STING-IRF3 and STING-NF-κB pathway after free and Nano ZSA-51D (10 and 100 nM) treatments for 4 hours in bone marrow derived macrophage from C57BL/6J mice.

(G) IFN-β, TNF-α and IL-6 secretion was measured using ELISA assay after free and Nano ZSA-51D (100 nM) treatments for 24 hours in bone marrow derived macrophage from C57BL/6J mice. Data are represented as mean ± SD. *$p < 0.05$, **$p < 0.01$, ***$p < 0.001$, ****$p < 0.0001$.

(H) Schematic of treatment schedule and flow cytometry analysis to assess neutrophil populations in tumors, bone marrow and blood of MC-38 tumor-bearing C57BL/6J mice at 24 hours post-treatment.

(I-K) Quantification (left) and representative flow cytometry plots (right) of neutrophils (NEs, $CD11b^{+}Ly\text{-}6G^{+}$) within $CD45^{+}$ immune cells in tumors (I), bone marrow(J) and blood (K) following free or Nano ZSA-51D treatment. Data are represented as mean ± SD (n = 3). *$p < 0.05$, **$p < 0.01$, ***$p < 0.001$, ****$p < 0.0001$, ns: not significant.

Nano ZSA-51D Expanded HSPCs and Skewed Differentiation Toward GMP

Neutrophils are derived from HSPCs in the bone marrow through a series of progressively restrictive differentiation steps (**Fig. S3**). To explore how Nano ZSA-51D reprograms HSPCs to expand neutrophil in vivo, we monitored the composition of HSPC subsets in bone marrow of

MC-38 tumor-bearing mice 24 hours after 3 doses administration (1 mg/kg, I.V.) by flow cytometric analysis (**Fig. 2A**).

Surprisingly , both free and Nano ZSA-51D treatments resulted in a marked expansion of the HSPCs ($Lin^{-}Sca\text{-}1^{+}c\text{-}Kit^{+}$, LSK) (**Fig. 2B**), which includes long-term hematopoietic stem cell (LT-HSC), short-term HSC (ST-HSC) and multipotent progenitor (MPP) (**Fig. 2C**).(*37*) Notably, MPP exhibited the most dramatic expansion, rising from 4.1% to 25.3%, indicating enhanced hematopoietic activity (**Fig. 2C)**. Among the MPP, the myeloid-biased multipotent progenitor 3 (MPP3) highly increased, while the lymphoid-biased multipotent progenitor 4 (MPP4) decreased correspondingly (**Fig. 2D**). In downstream progenitors, we also observed an increase in granulocyte-monocyte progenitor (GMP) (**Fig. 2E**). These results demonstrate that Nano ZSA-51D expanded HSPCs and skewed differentiation toward granulocyte-monocyte progenitors (GMP) to increase neutrophils and support innate immune responses (**Fig. 2F**).

Nano ZSA-51D Expanded HSPCs and Skewed Differentiation Toward GMP via STING-NF-κB-IL-6 Signaling

To elucidate how STING agonists can expand HSPCs and skew differentiation toward GMP, we isolated the LSK cells from the bone marrow of MC-38 tumor-bearing C57BL/6J mice and treated them with Nano ZSA-51D (100 nM) for 3 days in vitro (**Fig. 2G**). Interestingly, Nano ZSA-51D dramatically expanded HSPCs (LSK populations) from 18.1% to 76.3% (**Fig. 2H**), while vehicle-treated group showed HSPC differentiation. This observation suggests that STING activation can directly expand HSPCs at stem or multipotent progenitor state.

Since STING activation can induce different downstream cytokines such as IFN-β, TNF-α, and IL-6, we further test which of these cytokines can expand the HSPCs and skew differentiation toward GMP. We treated the isolated LSK cells with TNF-α, IFN-β, IFN-γ and IL-6 for 3 days and monitored the composition changes of HSPCs. Among these cytokines, only IL-6 expanded HSPCs (LSK population) (**Fig. 2I)** and significantly increased the GMP population (**Fig. 2J**). Given that IL-6 is a key downstream effector of the STING–NF-κB axis, these results suggest that Nano ZSA-51D initiates STING-NF-κB-IL-6 signaling to expand HSPCs, and skew differentiation toward the GMP.

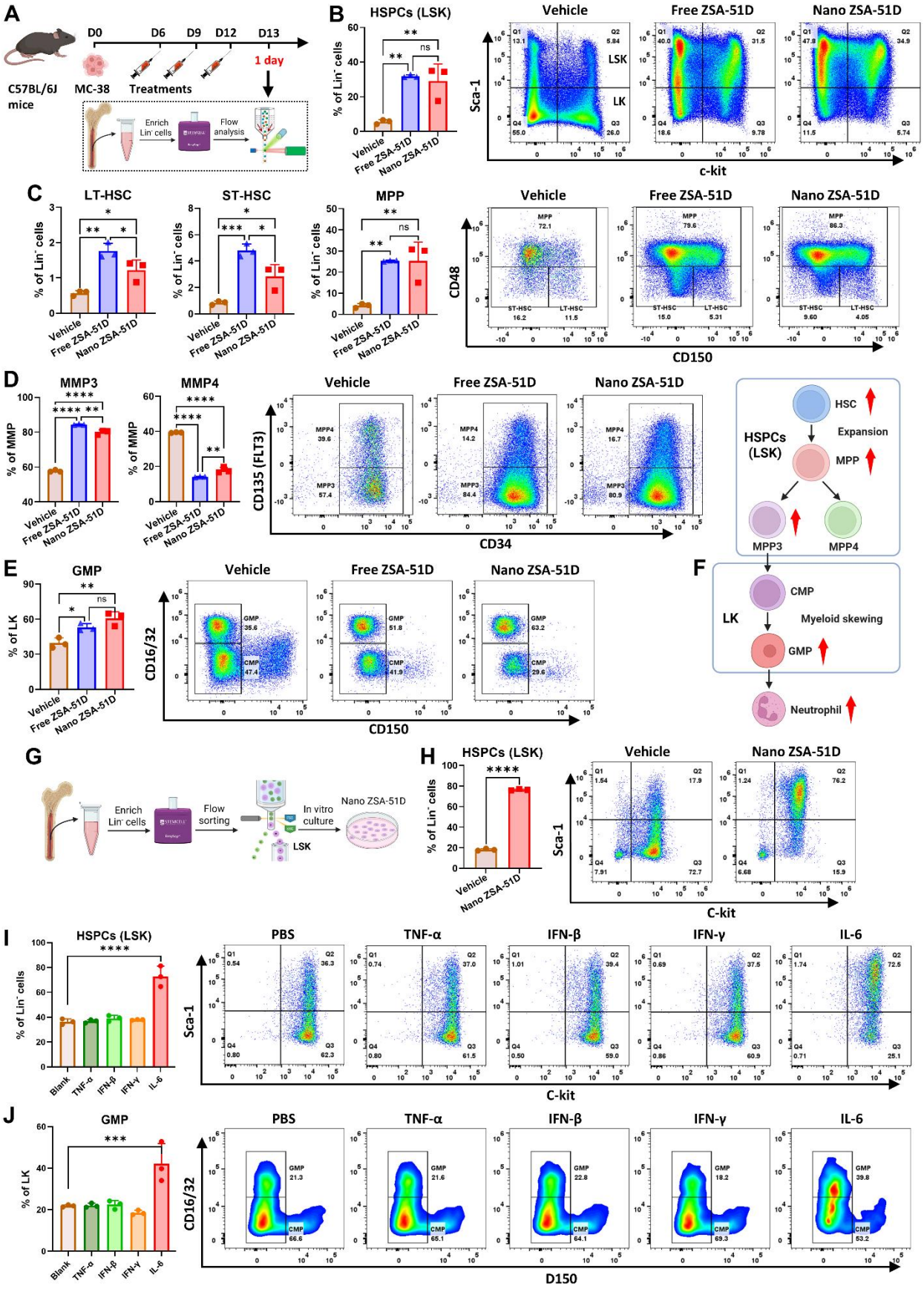
A
C57BL/6J mice
MC-38
Treatments
D0
D6
D9
D12
D13
1 day
Enrich Lin⁻ cells
Flow analysis
B
HSPCs (LSK)
% of Lin⁻ cells
Vehicle
Free ZSA-51D
Nano ZSA-51D
Sca-1
c-kit
LSK
LK
C
LT-HSC
ST-HSC
MPP
CD48
CD150
D
MMP3
MMP4
% of MMP
CD135 (FLT3)
CD34
HSPCs (LSK)
HSC
Expansion
MPP
MPP3
MPP4
E
GMP
% of LK
CD16/32
F
CMP
LK
Myeloid skewing
GMP
Neutrophil
G
Enrich Lin⁻ cells
Flow sorting
In vitro culture
Nano ZSA-51D
LSK
H
HSPCs (LSK)
% of Lin⁻ cells
Vehicle
Nano ZSA-51D
Sca-1
C-kit
I
HSPCs (LSK)
% of Lin⁻ cells
Blank
TNF-α
IFN-β
IFN-γ
IL-6
PBS
Sca-1
C-kit
J
GMP
% of LK
CD16/32
D150

1

Figure 2. Nano ZSA-51D expanded HSPCs and skewed differentiation toward GMP through STING-NF-κB-IL-6 Signaling.

(A) Schematic illustration of treatment schedule and flow cytometry analysis to examine the composition of HSPC subsets in bone marrow of MC-38 tumor bearing mice 24 hours post-treatment. The flow cytometry analysis of HSPCs was performed after enrichment of Lin^- cells.

(B) Quantification (left) and representative flow cytometry plots (right) of HSPCs ($Lin^-Sca\text{-}1^+c\text{-}Kit^+$, LSK) within Lin^- cells in bone marrow following free or Nano ZSA-51D treatment. Data are represented as mean ± SD (n = 3). $^{**}p < 0.01$, ns: not significant.

(C) Quantification (left) of LT-HSC ($CD150^+CD48^-$), ST-HSC ($CD150^-CD48^-$) and MPP ($CD150^{-/+}CD48^+$) within Lin^- cells and their representative flow cytometry plots (right) within LSK ($Lin^-Sca\text{-}1^+c\text{-}Kit^+$) in bone marrow following free or Nano ZSA-51D treatment. Data are represented as mean ± SD (n = 3). $^*p < 0.05$, $^{**}p < 0.01$, $^{***}p < 0.001$, ns: not significant.

(D) Quantification (left) and representative flow cytometry plots (right) of myeloid-biased multipotent progenitor 3 (MPP3, $CD34^+CD135^-$) and lymphoid-biased multipotent progenitor 4 (MPP4, $CD34^+CD135^+$) within MMP ($Lin^-Sca\text{-}1^+c\text{-}Kit^+CD150^{-/+}CD48^+$) in bone marrow following free or Nano ZSA-51D treatment. Data are represented as mean ± SD (n = 3). $^{****}p < 0.0001$, ns: not significant.

(E) Quantification (left) and representative flow cytometry plots (right) of granulocyte-monocyte progenitor (GMP, $CD150^-CD16/32^+$) within LK ($Lin^-Sca\text{-}1^-c\text{-}Kit^+$) in bone marrow following free or Nano ZSA-51D treatment. Data are represented as mean ± SD (n = 3). $^*p < 0.05$, $^{**}p < 0.01$, ns: no significance.

(F) Schematic illustration of HSPCs expansion and skewing differentiation toward GMP after STING agonist treatments. HSC, hematopoietic stem cell; MPP, multipotent progenitor; MPP3, myeloid-biased multipotent progenitor; MPP4, lymphoid-biased multipotent progenitor; CMP, common myeloid progenitor; GMP (granulocyte-monocyte progenitor).

(G) Experimental schematic of the in vitro treatment of LSK via Nano ZSA-51D (100 nM). The LSK ($Lin^-Sca\text{-}1^+c\text{-}Kit^+$) was sorted by flow after enrichment of Lin- cells from bone marrow cells.

(H) Quantification (left) and representative flow cytometry plots (right) of LSK ($Lin^-Sca\text{-}1^+c\text{-}Kit^+$) within Lin^- cells following in vitro treatment of Nano ZSA-51D for 3 days. Data are represented as mean ± SD (n = 3), $^{****}p < 0.0001$.

(I, J) Quantification (left) and representative flow cytometry plots (right) of HSPCs ($Lin^-Sca\text{-}1^+c\text{-}Kit^+$, LSK) within Lin^- cells (I) and GMP ($CD150^-CD16/32^+$) within LK ($Lin^-Sca\text{-}1^-c\text{-}Kit^+$) (J) following in vitro treatments of the STING pathway downstream cytokines (TNF-α, IFN-β, IFN-γ and IL-6) for 3 days. Data are represented as mean ± SD (n = 3), $^{***}p < 0.001$, $^{****}p < 0.0001$.

Nano ZSA-51D Reprograms Bone Marrow Neutrophils into $CD14^+ICAM\text{-}1^+$ Subsets that Enhanced Tumor Infiltration through STING–NF-κB–TNF-α Signaling

Recent studies have demonstrated that the immature/activated ($CD101^-CD14^+$) subset of tumor-infiltrating neutrophils is associated with improved responses to immunotherapy.(*32, 38-40*) CD101 is the maturation marker of neutrophils and CD14 is the activation marker of pattern recognition receptor-mediated immune responses.(*41-45*) To understand how Nano ZSA-51D further reprograms bone marrow neutrophils for tumor infiltration and antitumor activity, we

analyzed neutrophil subtypes in the bone marrow, peripheral blood, and tumors of MC-38 tumor-bearing mice 24 hours following STING agonist treatment.

In the bone marrow of vehicle-treated mice, most neutrophils were immature/inactivated ($CD101^{-}CD14^{-}$). Nano ZSA-51D treatment lead a 4-fold increase in immature/activated ($CD101^{-}CD14^{+}$) neutrophils from 7.5% to29.6 %, which was higher than free ZSA-51D treatment (**Fig. 3A**).

In the blood circulation of vehicle-treated mice, most neutrophils were mature/inactivated ($CD101^{+}CD14^{-}$) (**Fig. 3B)**. While Nano ZSA-51D treatment dramatically increased the immature/activated ($CD101^{-}CD14^{+}$) neutrophils from 0.08% to 20%, and mature/activated ($CD101^{+}CD14^{+}$) neutrophils from 9.1% to 47.2%, which were both substantially higher than free ZSA-51D treatment. These data suggest that Nano ZSA-51D strongly activated both immature and mature $CD14^{+}$ neutrophils, promoting their migration from bone marrow into bloodstream.

In the tumors, activated $CD14^{+}$ neutrophils preferentially infiltrated tumors following Nano ZSA-51D treatment. Specifically, the proportion of immature/activated $CD101^{-}CD14^{+}$ neutrophils increased from 2.0% to 11.2%, and mature/activated $CD101^{+}CD14^{+}$ neutrophils rose from 46.1% to 66.8% (**Fig. 3C**). This enhanced recruitment of $CD14^{+}$ neutrophils corresponded with the overall increase in tumor-infiltrating neutrophils (**Fig. 1I**). In contrast, although free ZSA-51D also expanded total neutrophil numbers in bone marrow and blood (**Fig. 1J and K**), it induced less $CD14^{+}$ subsets, resulting in less tumor infiltration. Therefore, Nano ZSA-51D effectively reprograms both immature and mature bone marrow neutrophils into activated $CD14^{+}$ subsets that enhance infiltration into tumors. In addition, we found that Nano ZSA-51D induced $CD14^{+}$ neutrophils highly expressed intercellular adhesion molecule-1 ($CD14^{+}ICAM\text{-}1^{+}$) in bone marrow and blood circulation (**Fig. 3D, E** and **Fig. S4A, B**), which promote $CD14^{+}ICAM\text{-}1^{+}$ neutrophil infiltration into tumor by interacting with integrins (e.g., LFA-1, Mac-1) expressed on endothelial cells (**Fig. 3F** and **Fig. S4C**).(*46, 47*)

To determine whether Nano ZSA-51D inducing $CD14^{+}ICAM\text{-}1^{+}$ neutrophils is mediated by STING pathway activation, we isolated bone marrow cells from wild-type (WT) C57BL/6J and STING deficient (C57BL/6J-Sting1gt/J) mice and treated them in vitro with free or Nano ZSA-51D (100 nM) for overnight. As expected, Nano ZSA-51D (100 nM) significantly increased both $CD101^{-}CD14^{+}$ and $CD101^{+}CD14^{+}$ neutrophil populations with high ICAM-1 expression

(CD14$^+$ICAM-1$^+$) from WT C57BL/6J mice, exceeding the effects observed with free ZSA-51D (**Fig. S5A, B**). However, bone marrow neutrophils from STING deficient mice failed to reprogram neutrophiles into CD101$^-$CD14$^+$, CD101$^+$CD14$^+$ and CD14$^+$ICAM-1$^+$ neutrophil populations, confirming the requirement of STING (**Fig. S5C, D**).

To further study which downstream mediators of STING signaling play a role in reprograming neutrophil subtypes, we treated the isolated bone marrow neutrophils with IFN-β, TNF-α, IL-6 and IFN-γ. We also used TGF-β as a control for immunosuppressive signaling. Among these, only TNF-α effectively reprogrammed bone marrow neutrophils into immature/activated (CD101$^-$CD14$^+$), mature/activated (CD101$^+$CD14$^+$) and CD14$^+$ICAM-1$^+$ subsets (**Fig. 3G-I and Fig. S6A, B**). Given that TNF-α is a key effector of STING-NF-κB axis, these findings suggest that Nano ZSA-51D reprograms immature and mature bone marrow neutrophils into CD14$^+$ICAM-1$^+$ subsets via STING-NF-κB-TNF-α signaling, enabling their infiltration into tumors (**Fig. 3J**).

Nano ZSA-51D-Induced CD14$^+$ Neutrophils Enhance Antitumor Response to α-PD1 Immunotherapy

To determine whether Nano ZSA-51D-induced CD14$^+$ bone marrow neutrophils possess antitumor immune activity, we isolated three neutrophil subsets from bone marrow cells treated with Nano ZSA-51D (100 nM) in vitro: immature/inactivated (CD101$^-$CD14$^-$), immature/activated (CD101$^-$CD14$^+$) and mature/activated (CD101$^+$CD14$^+$). Each subset was adoptively transferred intratumorally (I.T.) into MC-38 tumors in combination with α-PD1 therapy (**Fig. 3K**).

Interestingly, adoptive transfer of immature/activated (CD101$^-$CD14$^+$) neutrophils combined with α-PD1 achieved 100% tumor complete remission (100% CR) without recurrence, resulting in 100% long-term survival (**Fig. 3L, M and Fig. S7**). The mature/activated (CD101$^+$CD14$^+$) neutrophils also significantly enhanced anti-tumor efficacy, achieving a 60% CR rate. In contrast, the immature/inactivated (CD101$^-$CD14$^-$) neutrophils with α-PD1 did not significantly improve therapeutic outcomes compared to α-PD1 monotherapy. These findings suggest that Nano ZSA-51D-induced CD14$^+$ neutrophils possess potent antitumor properties that synergize with α-PD1 therapy.

To investigate whether the anti-tumor effect conferred by CD101$^-$CD14$^+$ neutrophils involved long-term immune memory, mice that achieved complete remission were rechallenged with MC-

38 tumor cells 120 days post-treatment (**Fig. S8A**). Notably, these mice completely resisted tumor re-growth (**Fig. S8B**), indicating the establishment of durable antitumor immune memory.

To further characterize the immune memory response, we analyzed $CD8^+$ and $CD4^+$ T cell memory subsets in the spleen, lymph nodes and blood of cured MC-38 mice at 180-day post-rechallenge (**Fig. S8A**). Flow cytometry analysis revealed a significant increase in $CD8^+$ T central memory (TCM) cells in cured MC-38 mice, with a 1.53-, 2.40- and 1.84-fold increase in spleen, lymph nodes and blood compared to naïve mice (**Fig 3N** and **Fig. S8C, E**). $CD4^+$ T effector memory (TEM) cells also increased in all tissues examined, while $CD4^+$ TCM cells remained unchanged (**Fig 3O** and **Fig. S8D, F**). These results demonstrate that adoptive transfer of $CD101^-CD14^+$ neutrophils with α-PD1 therapy promotes long-term $CD8^+$ T cell memory formation, contributing to complete tumor remission and long-lasting tumor immunity.

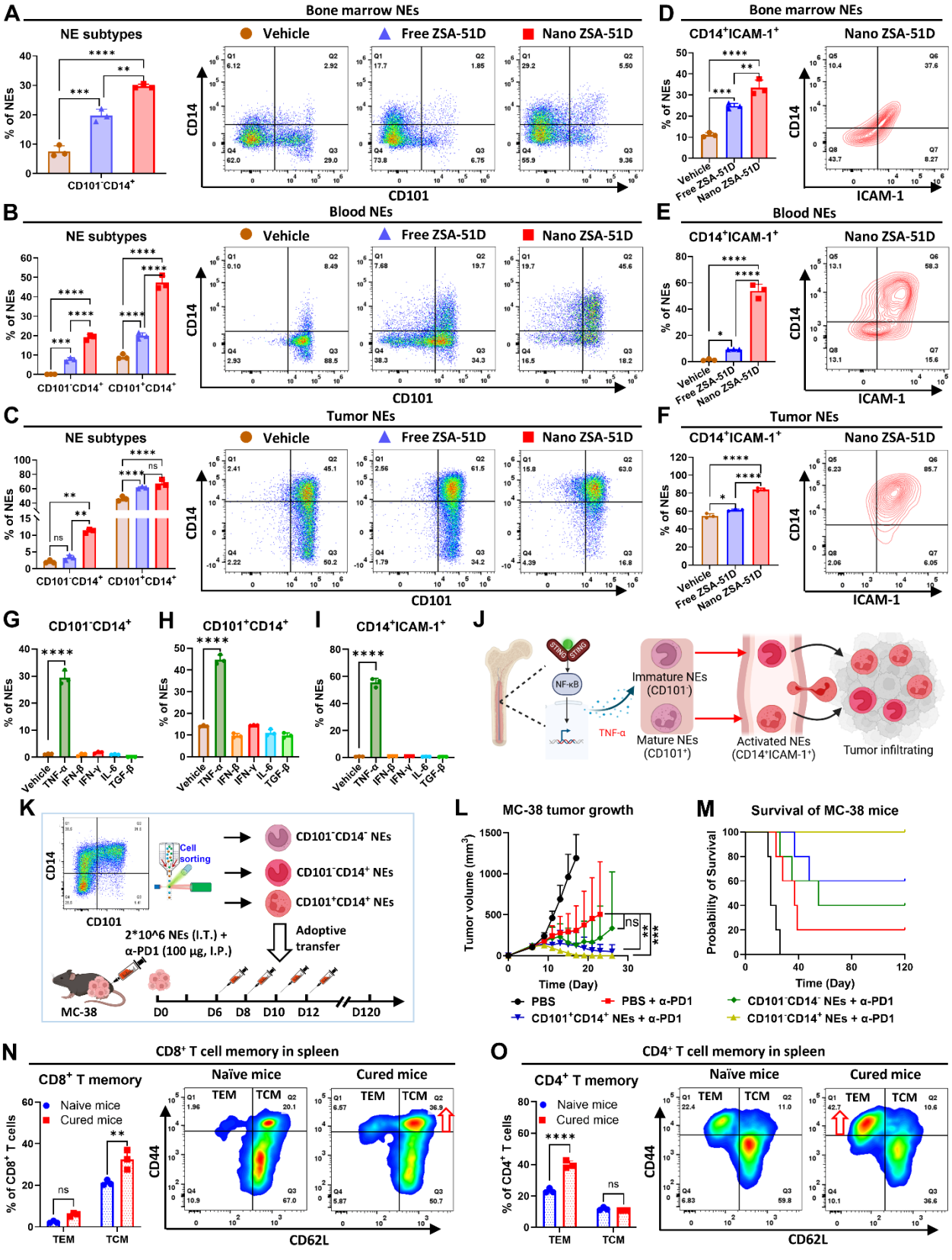
A
Bone marrow NEs
NE subtypes
Vehicle
Free ZSA-51D
Nano ZSA-51D
% of NEs
CD101⁻CD14⁺
CD14
CD101
B
Blood NEs
CD101⁻CD14⁺
CD101⁺CD14⁺
C
Tumor NEs
D
CD14⁺ICAM-1⁺
ICAM-1
E
F
G
CD101⁻CD14⁺
H
CD101⁺CD14⁺
I
CD14⁺ICAM-1⁺
Vehicle
TNF-α
IFN-β
IFN-γ
IL-6
TGF-β
J
STING
NF-κB
TNF-α
Immature NEs (CD101⁻)
Mature NEs (CD101⁺)
Activated NEs (CD14⁺ICAM-1⁺)
Tumor infiltrating
K
Cell sorting
CD101⁻CD14⁻ NEs
CD101⁻CD14⁺ NEs
CD101⁺CD14⁺ NEs
Adoptive transfer
2*10^6 NEs (I.T.) + α-PD1 (100 μg, I.P.)
MC-38
D0
D6
D8
D10
D12
D120
L
MC-38 tumor growth
Tumor volume (mm³)
Time (Day)
PBS
PBS + α-PD1
CD101⁻CD14⁻ NEs + α-PD1
CD101⁺CD14⁺ NEs + α-PD1
CD101⁻CD14⁺ NEs + α-PD1
M
Survival of MC-38 mice
Probability of Survival
Time (Day)
N
CD8⁺ T cell memory in spleen
CD8⁺ T memory
Naive mice
Cured mice
% of CD8⁺ T cells
TEM
TCM
CD44
CD62L
O
CD4⁺ T cell memory in spleen
CD4⁺ T memory
% of CD4⁺ T cells

1

Figure 3. Nano ZSA-51D reprogramed bone marrow neutrophils into $CD14^+ICAM\text{-}1^+$ subsets that enhanced tumor infiltration through STING–NF-κB–TNF-α signaling and synergizes with α-PD1 immunotherapy

(A-C) Quantification (left) and representative flow cytometry plots (right) showing the changes of $CD101^-CD14^+$ and $CD101^+CD14^+$ neutrophil (NE) subtypes in bone marrow (A), blood (B) and tumors (C) of MC-38 tumor-bearing C57BL/6J mice 24 hours after systemic administration of free and Nano ZSA-51D (1 mg/kg). Data are represented as mean ± SD (n = 3). **p < 0.01, ***p < 0.001, ****p < 0.0001, ns: not significant.

(D-F) Quantification (left) and representative flow cytometry plots (right) showing the changes of $CD14^+ICAM\text{-}1^+$ neutrophil subtypes in bone marrow (D), blood (E) and tumors (F) after systemic administration of Nano ZSA-51D (1 mg/kg). Data are represented as mean ± SD (n = 3). *p < 0.05, **p < 0.01, ***p < 0.001, ****p < 0.0001.

(G-I) Quantification of $CD101^-CD14^+$ (G), $CD101^+CD14^+$ (H) and $CD14^+ICAM\text{-}1^+$ (I) neutrophils following in vitro treatments of the STING pathway downstream cytokines (TNF-α, IFN-β, IFN-γ and IL-6) for overnight. The immunosuppressive TGF-β as control. Data are represented as mean ± SD (n = 3), ****p < 0.0001.

(J) Schematic illustration of STING activation-induced reprogramming of immature ($CD101^-$) and mature ($CD101^+$) bone marrow neutrophils into activated $CD14^+ICAM\text{-}1^+$ subsets with enhanced tumor infiltration.

(K) Schematic experiment of neutrophil adoptive transfer. $CD101^-CD14^-$, $CD101^-CD14^+$ and $CD101^+CD14^+$ neutrophils (NEs) were sorted from bone marrow cells pretreated overnight with Nano ZSA-51D (100 nM), then intratumorally injected into MC-38 tumor-bearing mice alongside intraperitoneal α-PD1 (100 μg/mouse).

(**L, M**) Tumor growth curves (L) and survival curves (M) of MC-38 tumor-bearing mice after adoptive transfer of $CD101^-CD14^-$, $CD101^-CD14^+$ or $CD101^+CD14^+$ neutrophils in combination with α-PD1 (100 μg/mice) treatments. Data are represented as mean ± SD (n=5). **p < 0.01, ***p < 0.001, ns: not significant. Survival comparisons were performed using a log-rank (Mantel–Cox) test.

(N, O) Quantification (left) and representative flow cytometry plots (right) of $CD8^+$ (N) and $CD4^+$ (O) effector memory (TEM: $CD62L^-CD44^+$) and central memory (TCM: $CD62L^+CD44^+$) T cells in the spleen of naïve C57BL/6J mice and cured mice at 180 day post-rechallenge. Data are represented as mean ± SD (n = 3), **p < 0.01, ****p < 0.0001, ns: not significant.

Nano ZSA-51D in Combination with α-PD1 Achieved Potent Therapeutic Efficacy in Colon and Pancreatic Cancer Models

Next, we evaluated the antitumor efficacy of Nano ZSA-51D in both MC-38 colon cancer and pancreatic cancer model (**Fig. 4A**). Notably, Nano ZSA-51D (1 mg/kg, I.V.) in combination with α-PD1 (100 μg/mice) achieved 100% tumor complete remission (100% CR) without recurrence, leading to 100% long-term survival (**Fig. 4B, C, Fig. S9**). By comparison, free ZSA-51D with α-

PD1 significantly inhibited tumor growth with 80% CR, while clinically tested STING agonist diABZI with 60% CR.

Furthermore, we evaluated the antitumor efficacy of Nano ZSA-51D in pancreatic ductal adenocarcinoma (PDAC) which is not response to PD-1 therapy. We used KPC 6422 and KPC 6620 cell lines, derived from the KPC (Kras^G12D, p53^R172H, Pdx1-Cre) genetically engineered mouse model of PDAC.(*48*) In both KPC 6422 and KPC 6620 pancreatic cancer models, Nano ZSA-51D (1 mg/kg, I.V.) with/without α-PD1 significantly reduced tumor burden and extend median survival, demonstrating superior efficacy over free ZSA-51D with/without α-PD1 (**Fig. 4D-G and Fig. S10, 11**). The Nano ZSA-51D at 2 mg/kg dose with α-PD1 led to significant tumor remission and extended median survival by 3 weeks compared to PD-1 monotherapy (**Fig. 4 F and G**). In the KPC 6422 model, tumor significant shrinkage and scabbing were observed after the 4th dose of Nano ZSA-51D (1 mg/kg, I.V.) with/without α-PD1 (**Fig. 4H**). In the 2 mg/kg Nano ZSA-51D plus α-PD1 group, tumor scabbing occurred after the 2nd doses and completely disappeared after the 4th dose, demonstrating rapid and effective tumor elimination.

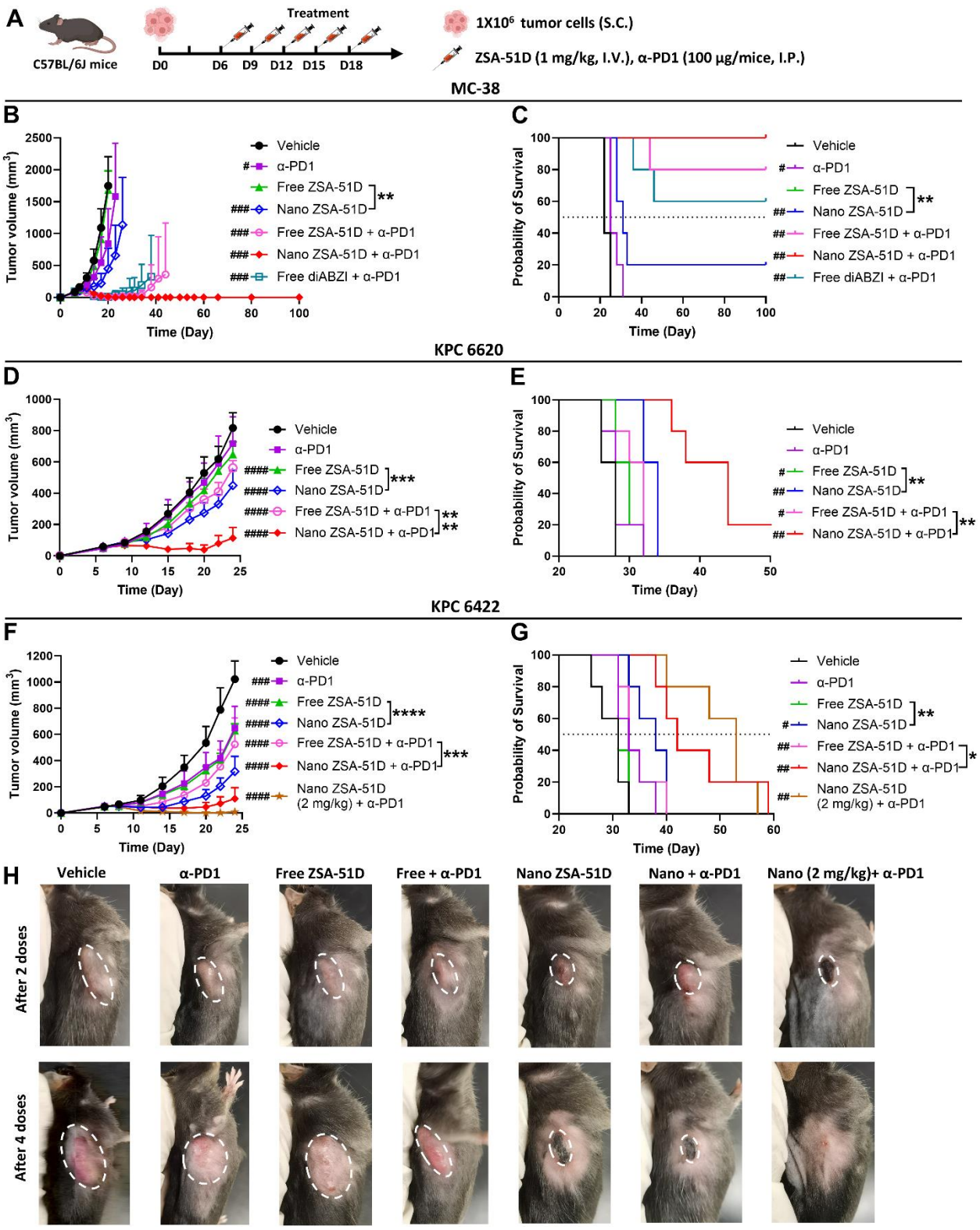

Figure 4. Nano ZSA-51D in combination with α-PD1 achieved potent anticancer therapeutic efficacy in colon and pancreatic cancer models.

(A) Schematic Illustration of the cancer model establishment in C57BL/6J mice and treatment regimen in tumor-bearing mice.
(B, C) Tumor growth curves (B) and survival curves (C) of MC-38 colon cancer cancer model following the indicated treatment regimens. Unless otherwise indicated, ZSA-51D or diABZI was administered at 1 mg/kg (I.V.) and α-PD1 at 100 μg/mouse (I.P.). Data are represented as mean ± SD (n = 5). **p < 0.01. #p < 0.05, ##p < 0.01, ###p < 0.001 vs. vehicle group.
(D, E) Tumor growth curves (D) and survival curves (E) of KPC 6620 pancreatic cancer model following the indicated treatment regimens. Data are represented as mean ± SD (n = 5). **p < 0.01, ***p < 0.001, ****p < 0.0001. #p < 0.05, ##p < 0.01, ####p < 0.0001 vs. vehicle group.
(F, G) Tumor growth curves (F) and survival curves (G) of KPC 6422 pancreatic cancer model following the indicated treatment regimens. Data are represented as mean ± SD (n = 5). *p < 0.05, **p < 0.01, ***p < 0.001, ****p < 0.0001. #p < 0.05, ##p < 0.01, ###p < 0.001, ####p < 0.0001 vs. vehicle group.
(H) Representative tumor images of the KPC 6422 pancreatic cancer model at 2 and 4 doses post-treatment. The white dashed line indicates tumor margin.

Nano ZSA-51D Induced Infiltration of $CD14^+$ Neutrophils and Promotes $CD8^+$ T cell Responses in TME

To further investigate how Nano ZSA-51D with/without α-PD1 therapy modulates the tumor immune microenvironment and induces an anticancer immune response, we analyzed tumor-infiltrating immune cells in MC-38 tumor-bearing mice using flow cytometry at 1- and 4-day post-treatment (**Fig. 5A**).

At 1-day post-treatment, Nano ZSA-51D without or with α-PD1 dramatically increased tumor-infiltrating neutrophils from 10.6% to 67% and 79.7% of $CD45^+$ immune cells, respectively, compared to vehicle-treated groups (**Fig. 5B and Fig. S12A**), as well as the immature/activated ($CD101^-CD14^+$) neutrophils from 0.22% to 6.4% and 13.5% (**Fig. 5C, E**), and the mature/activated ($CD101^+CD14^+$) neutrophils from 5% to 36.9% and 48.2% (**Fig. 5D, E**). In contrast, free ZSA-51D with/without α-PD1 also slightly enhanced total neutrophils and mature/activated ($CD101^+CD14^+$) neutrophils in tumors compared to vehicle-treated groups but did not significantly increase immature/activated ($CD101^-CD14^+$) neutrophils (**Fig. 5C-E)**. Conversely, 1-day post-treatment of Nano ZSA-51D with α-PD1 decreased macrophages from 59.7 % to 9.1 % of $CD45^+$ immune cells (**Fig. S12B, C**). A similar trend was also observed in the KPC 6620 pancreatic cancer model, where 1-day post-treatment of Nano ZSA-51D with α-PD1 increased

tumor-infiltrating neutrophils from 31.9% to 63.3% (**Fig. S13A, C**) and decreased macrophages from 55.1% to 21.7% (**Fig. S13B, D**).

However, at 4-day post-treatment, tumor-infiltrating neutrophils significantly declined compared to 1-day post-treatment, with the most substantial reduction observed from 79.7% to 20.4% in the Nano ZSA-51D with α-PD1 (**Fig. 5F and Fig. S14A**).

Concurrently, at 4-day post-treatment, Nano ZSA-51D with/without α-PD1 significantly increased tumor-infiltrating $CD3^+$ T cells, with the most dramatic increase from 11.1% to 35.9% of $CD45^+$ immune cells in Nano ZSA-51D with α-PD1 group, which is significantly higher than that of free ZSA-51D with/without α-PD1 (**Fig. 5G and Fig. S14B**). Further analysis revealed that Nano ZSA-51D with/without α-PD1 expanded tumor-infiltrating $CD8^+$ T cells, while tumor-infiltrating $CD4^+$ T cell proportions remained unchanged among $CD45^+$ immune cells **(Fig. 5H-J)**. These results suggested that Nano ZSA-51D promoted $CD8^+$ T cell responses following infiltration of immature and mature activated $CD14^+$ neutrophils in the TME.

To assess whether Nano ZSA-51D with α-PD1 therapy generates tumor-specific immune memory, we performed tumor rechallenge experiments in cured MC-38 mice 100 days post-treatment (**Fig. 5K**). MC-38 tumor cells failed to establish tumors in Nano ZSA-51D with α-PD1 cured MC-38 mice, while KPC 6422 tumors grew at similar rates in both naïve and cured MC-38 mice (**Fig. 5L, M**). These results suggest that Nano ZSA-51D with α-PD1 therapy induced a tumor-specific immune memory response against MC-38 tumor cells but not against KPC 6422 tumor cells.

To further characterize the immune memory response, we also analyzed $CD8^+$ and $CD4^+$ T cell memory subsets in the spleen, lymph nodes and blood of cured MC-38 mice 180 days after tumor rechallenge (**Fig. 5K**). Flow cytometry analysis revealed a significant increase in $CD8^+$ T central memory (TCM) cells in cured MC-38 mice, with a 3.3-, 4.4- and 4.5-fold increase in spleen, lymph nodes and blood compared to naïve mice (**Fig. 5N and Fig. S15A, C**). While $CD4^+$ TCM cells had no significant change (**Fig. 5O and Fig. S15B, D**). These results further confirmed that Nano ZSA-51D with α-PD1 therapy also generated the long term $CD8^+$ T cell memory, which contributed to complete tumor remission and long-lasting tumor immunity.

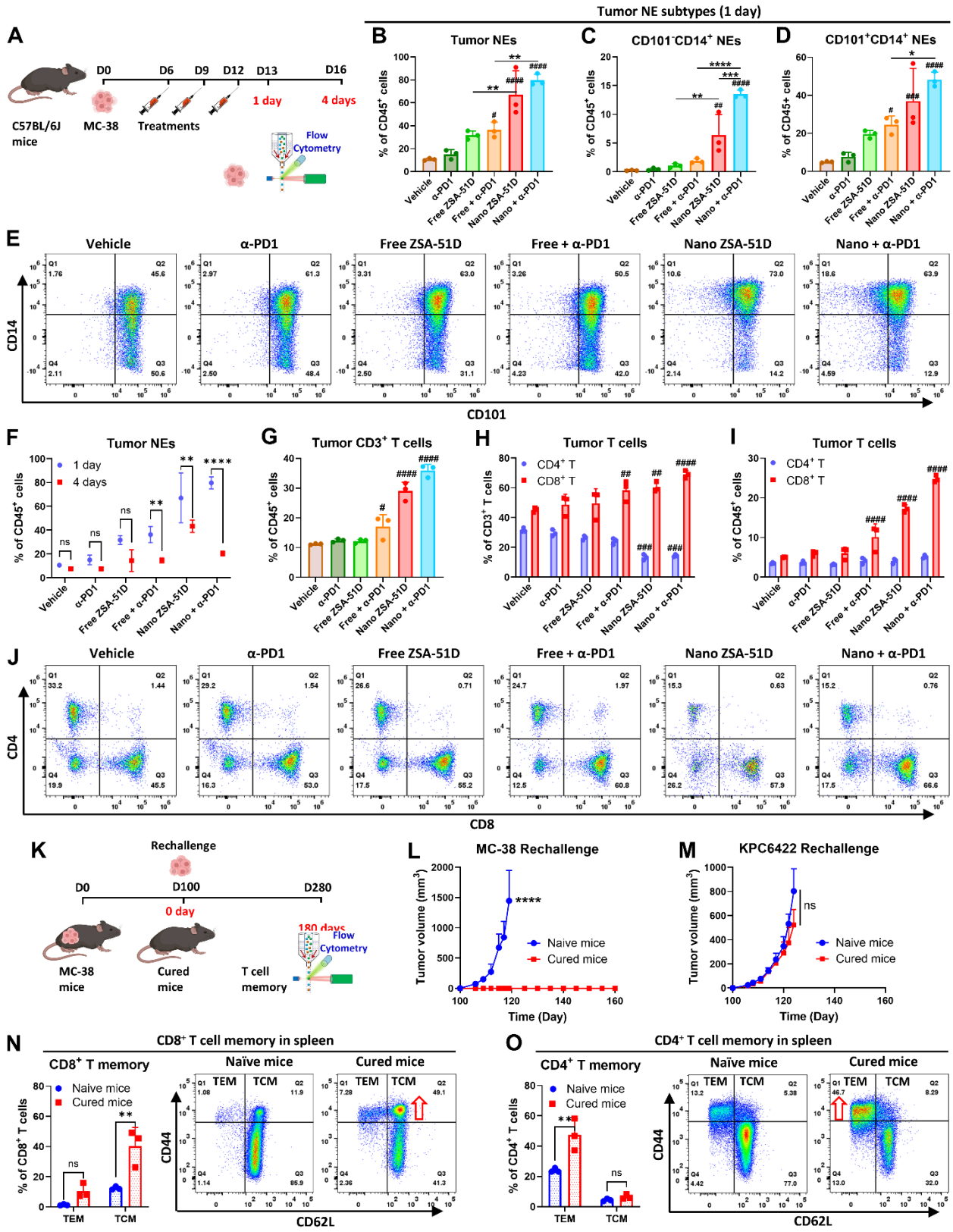
A
D0
D6
D9
D12
D13
D16
1 day
4 days
C57BL/6J mice
MC-38
Treatments
Flow Cytometry
Tumor NE subtypes (1 day)
B
Tumor NEs
C
CD101⁻CD14⁺ NEs
D
CD101⁺CD14⁺ NEs
% of CD45⁺ cells
Vehicle
α-PD1
Free ZSA-51D
Free + α-PD1
Nano ZSA-51D
Nano + α-PD1
E
CD14
CD101
F
Tumor NEs
1 day
4 days
% of CD45⁺ cells
G
Tumor CD3⁺ T cells
H
Tumor T cells
CD4⁺ T
CD8⁺ T
% of CD3⁺ T cells
I
Tumor T cells
J
CD4
CD8
K
Rechallenge
D0
D100
D280
0 day
180 days
MC-38 mice
Cured mice
T cell memory
L
MC-38 Rechallenge
Tumor volume (mm³)
Naive mice
Cured mice
Time (Day)
M
KPC6422 Rechallenge
N
CD8⁺ T cell memory in spleen
CD8⁺ T memory
Naïve mice
Cured mice
% of CD8⁺ T cells
TEM
TCM
CD44
CD62L
O
CD4⁺ T cell memory in spleen
CD4⁺ T memory
% of CD4⁺ T cells

1

Figure 5. Nano ZSA-51D induced infiltration of activated $CD14^+$ neutrophils and triggered $CD8^+$ T cell responses in TME.

(A) Schematic illustrating the treatment schedule and flow cytometry analysis of tumor-infiltrating immune cells in MC-38 tumor-bearing C57BL/6J mice at 1 day and 4 days post-treatment.

(B-D) Quantification of total tumor-infiltrating neutrophils (NEs) (B), $CD101^-CD14^+$ (C) and $CD101^+CD14^+$ (D) NEs within $CD45^+$ immune cells at 1-day post-treatment. Data are represented as mean ± SD (n = 3). *p < 0.05, **p < 0.01, ***p < 0.001, ****p < 0.0001; #p < 0.05, ##p < 0.01, ###p < 0.001, ####p < 0.0001 vs. vehicle group.

(E) Representative flow cytometry plots showing the changes of $CD101^-CD14^+$ and $CD101^+CD14^+$ neutrophils in tumors at 1-day post-treatment.

(F) Quantification and comparison of tumor-infiltrating neutrophils within $CD45^+$ immune cells at 1 day and 4 days post-treatment. Data are represented as mean ± SD (n = 3). **p < 0.01, ****p < 0.0001.

(G-I) Quantification of $CD3^+$ T cells within $CD45^+$ immune cells (G), $CD4^+$ and $CD8^+$ T cells within $CD3^+$ T cells (H) or within $CD45^+$ immune cells (I) at 4 days post-treatment. Data are represented mean ± SD (n = 3). #p < 0.05, ##p < 0.01, ###p < 0.001, ####p < 0.0001 vs. vehicle group.

(J) Representative flow cytometry plots showing tumor-infiltrating $CD4^+$ and $CD8^+$ T cells within $CD3^+$ T cells at 4 days post-treatment.

(K) Schematic of MC-38 tumor cell rechallenge in mice cured with Nano ZSA-51D and α-PD1 combination therapy at 100 days post-treatment. Long-term T cell memory was evaluated by flow cytometry at 180 day post-rechallenge.

(**L, M**) Tumor growth curves following rechallenge with MC-38 (L) or KPC 6422 (M) tumor cell in naïve C57BL/6J mice and cured mice at 100 days post-treatment. Data are represented as mean ± SD (n=5). ****p < 0.0001; ns, not significant.

(N, O) Quantification (left) and representative flow cytometry plots (right) of $CD8^+$ (N) and $CD4^+$ (O) effector memory (TEM: $CD62L^-CD44^+$) and central memory (TCM: $CD62L^+CD44^+$) T cells in the spleen of naïve C57BL/6J mice and cured mice at 180-day post-rechallenge. Data are represented as mean ± SD (n=3). **p < 0.01; ns, not significant.

Nano ZSA-51D Induced $CD14^+$ Neutrophils with Enhanced MHC I Antigen Presentation Capacity

To further elucidate how Nano ZSA-51D-induced $CD14^+$ tumor neutrophil infiltration contributes to $CD8^+$ T cell responses, we performed bulk mRNA sequencing on sorted total neutrophils and their subtypes from bone marrow cells following Nano ZSA-51D (100 nM) treatment in vitro. Differential gene expression analysis revealed that anti-tumor neutrophil (N1) markers were

upregulated, while pro-tumor (N2) markers were downregulated following treatment, indicating a shift toward an N1-like neutrophil phenotype(*49-51*) (**Fig. 6A**).

Moreover, the interferon-stimulated genes (ISGs) were highly upregulated in neutrophils following Nano ZSA-51D treatment (**Fig. 6B**). Previous studies suggest that ISG expression is associated with antigen presentation machinery, serving as a crucial bridge between innate and adaptive immunity.(*52, 53*) GO Gene set enrichment analysis (GSEA) further revealed significant enrichment of the gene response to IFN-β (NES = 2.83, FDR q = 2.23E-21) in Nano ZSA-51D treated neutrophils (**Fig. 6C**), indicating that STING pathway activation drives IFN-β–mediated transcriptional programming in these cells.

KEGG pathway enrichment analysis identified the top 20 hallmark pathways altered in neutrophils by Nano ZSA-51D (**Fig. 6D**). Among them, the key innate immune signaling pathways were highly enriched and upregulated, including Cytosolic DNA-sensing, NOD-like receptor, toll-like receptor and C-type lectin receptor pathways, along with their downstream signaling cascades such as the TNF and NF-kappa B pathways (**Fig. 6E and Fig. S16A, B**). These pathways play critical roles in enabling the $CD14^+$ neutrophils to detect pathogen-associated molecular patterns (PAMPs) and damage-associated molecular patterns (DAMPs) in the TME.(*54-57*)

A striking finding was the significant enrichment and upregulation of antigen processing and presentation pathway (NES = 2.00, FDR q = 4.36E-5) in neutrophils by Nano ZSA-51D treatment (**Fig. S16C)** as well as immature/activated ($CD101^-CD14^+$) (NES = 2.03, FDR q = 3.49E-5) and mature/activated ($CD101^+CD14^+$) (NES = 2.1, FDR q = 2.24E-6) neutrophils **(Fig. 6E)**. Further GO GSEA analysis confirmed that MHC class I-mediated antigen processing and presentation were highly upregulated in $CD101^-CD14^+$ (**Fig. 6F)** and $CD101^+CD14^+$ (**Fig. 6G)** neutrophils, along with MHC class I protein complex assembly (**Fig. S16D, E**). In contrast, MHC class II-mediated antigen processing and presentation and MHC class II protein complex assembly remained unchanged (NES < 1.5, FDR q > 0.05).

Consistently, Nano ZSA-51D markedly upregulated the expression of MHC class I subunits, costimulatory ligands, T cell-activating cytokines and T cell-recruiting chemokines in these neutrophils, further reinforcing their antigen-presenting potential **(Fig. 6H)**. In contrast, MHC class II subunit expression remained unchanged **(Fig. S16F**).

To functionally confirm MHC class I antigen presentation by Nano ZSA-51D induced immature and mature $CD14^+$ neutrophils, we performed flow cytometry analysis on bone marrow neutrophils treated with Nano ZSA-51D and/or OT-I peptide (CSSSIINFEKL from OVA). Nano ZSA-51D significantly upregulated MHC class I expression on neutrophils with or without OT-I peptide (**Fig. 6I**), while MHC class II expression remained unchanged (**Fig. 6J**). Importantly, MHC class I presentation of OT-I peptide (H-$2K^b$ OT-I complex) was greatly enhanced 3.6-fold on neutrophils after Nano ZSA-51D treatment (**Fig. 6K**). Both immature/activated ($CD101^-CD14^+$) and mature/activated ($CD101^+CD14^+$) neutrophils demonstrated superior antigen presenting capacity compared to untreated control (**Fig. 6L**). These results suggest that Nano ZSA-51D induced immature and mature $CD14^+$ neutrophils with enhanced MHC I-mediated antigen-presenting capacity, potentially enabling effective priming of $CD8^+$ T cell immunity (**Fig. 6M**).

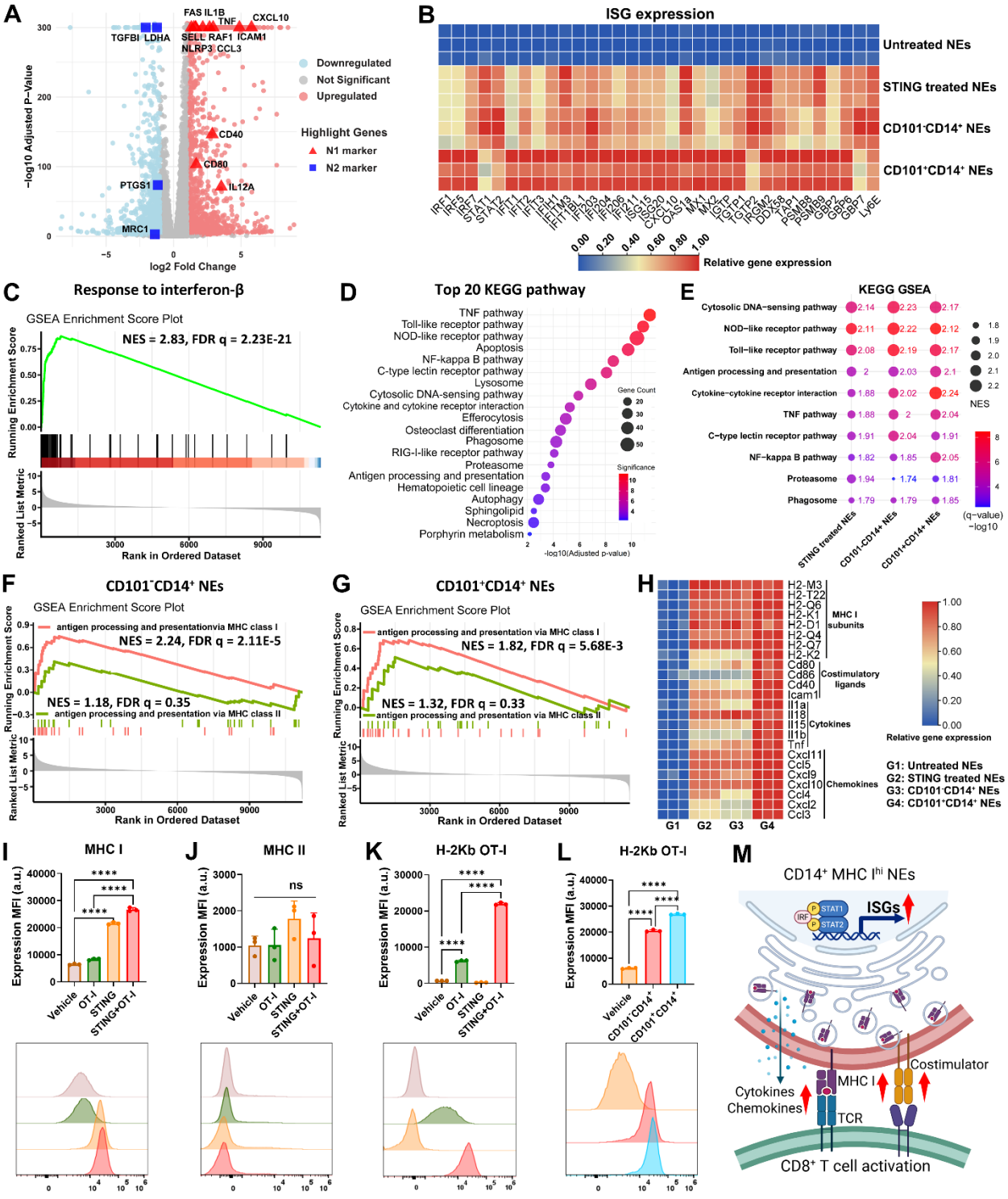

Figure 6. Nano ZSA-51D induced CD14⁺ neutrophils with enhanced MHC I antigen presentation capacity.

(A) Volcano plot of differentially expressed gene analysis between vehicle and Nano ZSA-51D treated neutrophils. Significance threshold for P adjusted value was 0.01 and foldchange was 2. The anti- (N1, red triangle) and pro- (N2, blue square) tumorigenic neutrophil markers were highlighted.

(B) Heatmap of relative interferon-stimulated gene (ISG) expression in Nano ZSA-51D-treated neutrophils (NEs) and their $CD101^{-}CD14^{+}$ and $CD101^{+}CD14^{+}$ subtypes, compared to untreated neutrophils.

(C) Gene Ontology (GO) GESA enrichment score plots for biological process that response to interferon-beta (IFN-β) in Nano ZSA-51D treated neutrophils.

(D) Top 20 KEGG pathway enrichment analysis based on the differentially expressed genes (DEGs) in neutrophils from Nano ZSA-51D-treated and vehicle-treated groups, ranked by adjusted p-values.

(E) Top 10 upregulated pathways in Nano ZSA-51D-treated neutrophils and their $CD101^{-}CD14^{+}$ and $CD101^{+}CD14^{+}$ subtypes, identified by KEGG Gene Set Enrichment Analysis (GESA). Normalized enrichment score (NES > 1.5) indicates significant upregulation. FDR q-value ($q < 0.05$) denotes statistical significance after false discovery rate adjustment.

(**F, G**) Gene Ontology (GO) GESA enrichment score plots for antigen processing and presentation via MHC class I and II in $CD101^{-}CD14^{+}$ (B) and $CD101^{+}CD14^{+}$ (C) neutrophils. Normalized enrichment score (NES > 1.5) indicates significant upregulation. FDR q-value ($q < 0.05$) denotes statistical significance after false discovery rate adjustment.

(H) Heatmap of relative gene expression of MHC class I subunits, costimulatory ligands, T cell-activating cytokines and T cell-recruiting chemokines in Nano ZSA-51D-treated neutrophils and their $CD101^{-}CD14^{+}$ and $CD101^{+}CD14^{+}$ subtypes.

(**I, J**) Protein expression of MHC class I and II molecules on bone marrow neutrophils following treatments with OT-I or/and Nano ZSA-51D. Data are represented as mean ± SD (n = 3). ****$p < 0.0001$, ns: not significant.

(**K**) presentation of OT-I peptide via MHC class I (H-$2K^{b}$-OT-I complex) on neutrophils following treatments with OT-I or/and Nano ZSA-51D. Data are represented as mean ± SD (n = 3). ****$p < 0.0001$.

(**L**) presentation of OT-I peptide via MHC class I (H-$2K^{b}$-OT-I complex) on $CD101^{-}CD14^{+}$ and $CD101^{+}CD14^{+}$ neutrophils following OT-I treatment. Data are represented as mean ± SD (n = 3). ****$p < 0.0001$.

(M) Schematic illustration of antigen presentation by ISG-expressing $CD14^{+}$MHC I^{hi} neutrophils via MHC class I to activate $CD8^{+}$ T cells.

Nano ZSA-51D-Induced $CD14^{+}$ Neutrophils Prime Antigen-Specific $CD8^{+}$ T Cell Immunity

To investigate whether Nano ZSA-51D-Induced $CD14^{+}$ neutrophils can effectively prime antigen-specific $CD8^{+}$ T cell activation and proliferation via MHC I-mediated antigen presentation, we

conducted a co-culture experiment using OT-I $CD8^+$ T cells from transgenic OT-I mice. We sorted total neutrophils from bone marrow cells that pre-treated with ovalbumin (OVA, 0.2 mg/mL) and Nano ZSA-51D (100 nM), and co-incubated them with OT-I $CD8^+$ T cells for 48 hours (**Fig. 7A**).

Strikingly, neutrophils treated with OVA and Nano ZSA-51D induced extensive OT-I $CD8^+$ T cell clustering (**Fig. 7B**), suggesting enhanced recruitment, activation, and proliferation of OT-I $CD8^+$ T cells. Flow cytometry analysis further confirmed that OVA and Nano ZSA-51D co-treated neutrophils strongly activated OT-I $CD8^+$ T cells, as indicated by a significant increase in CD69, CD25 and CD137 (4-1BB) expression (**Fig. 7 C and Fig. S17A, B**). Moreover, they significantly promoted the proliferation of OT-I $CD8^+$ T cells, as demonstrated by flow cytometry proliferation assays (**Fig. 7D**). These data suggested Nano ZSA-51D-treated bone marrow neutrophils activated $CD8^+$ T cell immunity through enhanced MHC-I antigen presentation.

To assess the $CD8^+$ T cell activation potential of immature and mature $CD14^+$ neutrophils, we sorted these two distinct neutrophil subtypes from bone marrow cells that treated with OVA and Nano ZSA-51D, and co-incubated them with OT-I $CD8^+$ T cells for 48 hours. Both immature/activated ($CD101^-CD14^+$) and mature/activated ($CD101^+CD14^+$) neutrophils treated with OVA and Nano ZSA-51D induced prominent OT-I $CD8^+$ T cell clustering (**Fig. 7E**). Further Flow cytometry analysis revealed that both $CD101^-CD14^+$ and $CD101^+CD14^+$ neutrophils strongly activated OT-I $CD8^+$ T cells, as indicated by increased expression of CD69, CD25, and CD137 (4-1BB) (**Fig. 7 F and Fig. S17C, D**) and significantly promoted OT-I $CD8^+$ T cell proliferation (**Fig. 7 G**). These results demonstrated that Nano ZSA-51D-Induced immature/ activated ($CD101^-CD14^+$) and mature/activated ($CD101^+CD14^+$) neutrophils mediated potent antigen-specific $CD8^+$ T cell activation and proliferation.

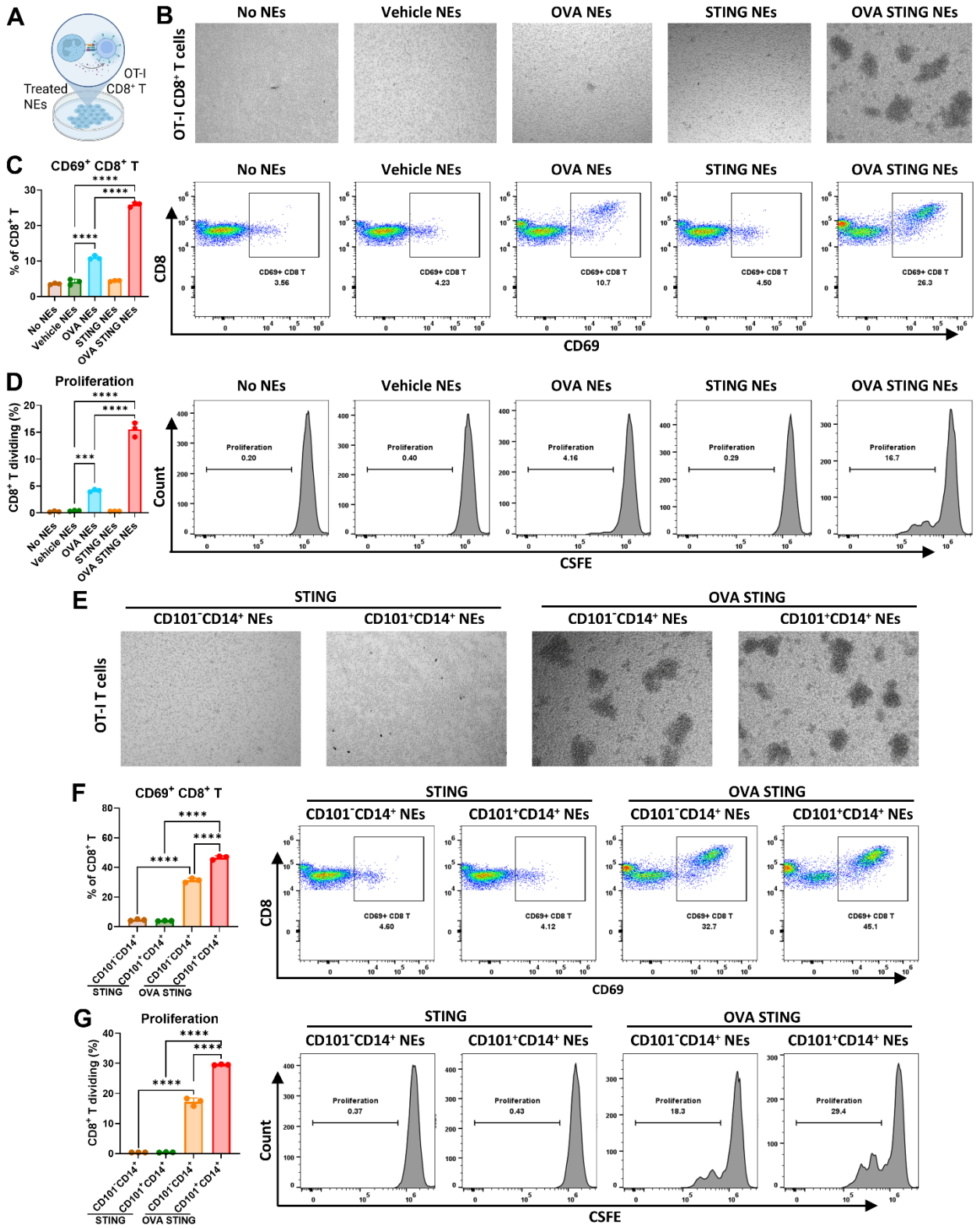

Figure 7. Nano ZSA-51D-induced CD14+ neutrophils prime CD8+ T cells via MHC I antigen presentation.

(A) Experimental schematic showing Nano ZSA-51D (100 Nm) and OVA (0.2 mg/ml) pre-treated neutrophils (NEs) co-incubated with OT-I $CD8^+$ T cells for 48 hours.
(B) Bright-field microscopy images of OT-I $CD8^+$ T cells after co-incubation with differently treated bone marrow neutrophils (NEs) for 48 hours. Neutrophils were sorted from bone marrow pretreated overnight with OVA (0.2 mg/ml) or/and Nano ZSA-51D (100 nM).
(C) Quantification (left) and representative flow cytometry plots (right) of $CD69^+$ OT-I $CD8^+$ T cell activation after co-incubation with differently treated neutrophils for 48 hours. Data are represented as mean ± SD (n = 3). ****$p < 0.0001$; ####$p < 0.0001$ vs. vehicle-treated neutrophils.
(D) Quantification (left) and representative flow cytometry plots (right) of OT-I $CD8^+$ T cell proliferation by CSFE staining after co-incubation with differently treated neutrophils for 48 hours. Data represent mean ± SD (n=3). ****$p < 0.0001$; ####$p < 0.0001$ vs. vehicle-treated neutrophils.
(E) Bright-field microscopy images of OT-I CD8+ T cells after co-incubation with differently treated IA ($CD101^-CD14^+$) and MA ($CD101^+CD14^+$) neutrophils for 48 hours. IA ($CD101^-CD14^+$) and MA ($CD101^+CD14^+$) neutrophils were sorted from bone marrow pretreated overnight with Nano ZSA-51D (100 nM) with or without OVA.
(F) Quantification (left) and representative flow cytometry plots (right) of $CD69^+$ OT-I $CD8^+$ T cell activation after co-incubation with differently treated IA (CD101-CD14+) and MA (CD101+CD14+) neutrophils for 48 hours. Data are represented as mean ± SD (n=3). ****$p < 0.0001$; ####$p < 0.0001$ vs. respective neutrophil subtype control.
(G) Quantification (left) and representative flow cytometry plots (right) of OT-I $CD8^+$ T cell proliferation by CSFE staining after co-incubation with differently treated IA (CD101-CD14+) and MA (CD101+CD14+) neutrophils for 48 hours. Data are represented as mean ± SD (n=3). ****$p < 0.0001$; ####$p < 0.0001$ vs. respective neutrophil subtype control.

DISCUSSION

Although STING pathway activation is a powerful strategy for triggering innate and anti-tumor immune responses, most studies have focused on its effects in dendritic cells and macrophages.(*2-4*) Neutrophils, despite being the most abundant innate immune cells, have long been considered immunosuppressive in the tumor microenvironment and largely excluded from STING-related therapeutic strategies.(*14*) However, recent evidence suggests that neutrophils can be reprogrammed from HSPCs into antitumor phenotypes.(*30*) Critically, how STING agonists regulate HSPCs and reprogram them into different neutrophil phenotypes to promote anti-tumor immunity remains unknown.

In this study, we developed a novel systemically administered dimeric STING agonist encapsulated into an albumin nanocomplex, Nano ZSA-51D, which expanded HSPCs and

reprogram them to anticancer neutrophils with enhanced MHC I antigen presentation to activate $CD8^+$ T cell antitumor immunity. We proved that Nano ZSA-51D combined with α-PD1 achieved potent anticancer efficacy in colon and pancreatic cancer models with minimal toxicity.

While prior studies have mainly focused on STING-induced activation of dendritic cells and macrophages, our work significantly broadens this paradigm by reprograming HSPCs to anticancer neutrophils as key effector cells in STING-based immunotherapy. Our findings reveal that Nano ZSA-51D expanded HSPCs and skewed their differentiation toward granulocyte-monocyte progenitors (GMP) through STING–NF-κB–IL-6 signaling, eventually expanding the neutrophil lineage. This suggests that STING signaling in the bone marrow is not merely an immune-sensing pathway but also a potent regulator of hematopoietic fate decisions. Mechanistically, NF-κB activation downstream of STING may drive IL-6 production, creating a cytokine milieu that favors granulocyte-monocyte lineage commitment. IL-6, in turn, has been reported to enhance the proliferation of granulocyte-monocyte progenitors and promote granulopoiesis, aligning with our observed increase in neutrophil output.(*58*) By reprograming HSPCs toward generating antitumor neutrophils, Nano ZSA-51D may establish a granulocyte-monocyte biased immune landscape that is preconfigured for rapid tumor recognition and support of adaptive immunity. This is conceptually aligned with recent evidence that microbial cancer immunotherapy reprograms HSPCs to amplify myelopoiesis, leading to increased production of neutrophils, monocytes, and dendritic cells that enhance antigen presentation and stimulate T cell–dependent antitumor immunity.(*30*)

Furthermore, this study uncovered a previously underexplored antitumor role of neutrophils in STING-mediated cancer immunotherapy. We showed that both immature ($CD101^-$) and mature ($CD101^+$) bone marrow neutrophils were reprogrammed into $CD14^+ICAM\text{-}1^+$ subsets via STING–NF-κB–TNF-α signaling by Nano ZSA-51D. These $CD14^+ICAM\text{-}1^+$ neutrophils infiltrated tumors more effectively and exhibited potent synergy with anti-PD1 therapy. Notably, adoptive transfer of Nano ZSA-51D-induced immature $CD14^+$ neutrophils in combination with α-PD1 led to complete tumor remission and the establishment of long-term $CD8^+$ T cell central memory, highlighting their potent anti-tumor immune function. The cell surface antigen CD14 is primarily understood to act as a co-receptor for toll-like receptors to activate innate immunity responses to pathogens by binding to PAMPs and DAMPs.(*44, 59-61*) While neutrophil ICAM-1 (CD54) expression correlated with enhanced migration and phagocytosis.(*46, 47, 62*) The acquisition of

CD14 and ICAM-1 on neutrophils may endow them with increased responsiveness to PAMPs and DAMPs within the tumor microenvironment, contributing to their improved antigen-presenting capacity, tumor infiltration, and their ability to activate innate and adaptive immunity in synergy with immune checkpoint blockade.

The transcriptomic and immune profiling revealed that Nano ZSA-51D-induced $CD14^+$ neutrophils upregulated ISG expression in responsive to IFN-β and exhibited high MHC class I expression. This conferred them with enhanced MHC class I antigen presenting capacity, thereby supporting antigen-specific $CD8^+$ T-cell-mediated antitumor immunity and bridging innate and adaptive immunity in TME. Previous studies have identified a subset of ICAM-$1^{hi}CD14^+$MHC I^{hi} APC-like "hybrid neutrophils", derived from immature progenitors, that are capable of cross-presenting antigens and initiating robust anti-tumor T cell responses in early-stage human lung cancer.(*38, 39*) In contrast, $CD11b^+CD14^-$ MDSCs have been shown to exert immunosuppressive effects on $CD8^+$ T cells, contributing to immune evasion in non-small cell lung cancer.(*40*) Collectively, these findings suggest that Nano ZSA-51D-induced $CD14^+$ICAM-1^+MHC I^{hi} neutrophils adopt an antitumor phenotype, distinct from immunosuppressive PMN-MDSCs.

Finally, despite extensive efforts to develop STING agonists that mimic natural CDNs, their clinical efficacy has been limited.(*63-65*) These CDN-based STING agonists suffer from rapid enzymatic degradation and poor cellular permeability due to their hydrophilic and anionic nature, restricting their use to intratumoral administration and limiting their impact on distant and metastatic lesions. To overcome these limitations, nanoparticle-based CDNs and non-CDN STING agonists with improved pharmacological properties have been developed for systemic bioavailability, demonstrating potent antitumor activity.(*33, 65-69*) Our albumin-STING agonist nanocomplex Nano-51D not only had unique anticancer efficacy as discussed above but also showed low toxicity. We evaluate the safety profile of Nano ZSA-51D by conducting comprehensive toxicity evaluations at 3 days post-treatment with single and multiple doses (5 doses, 1 mg/kg, I.V.). Complete blood cell count, liver functions, and histopathological assessments revealed no significant toxicity (Fig. S18), indicating that Nano ZSA-51D is well tolerated.

In summary, we demonstrate that albumin-STING agonist nanocomplex Nano ZSA-51D expanded HSPCs and reprogrammed them into antitumor neutrophils that migrate from bone marrow to

TME for enhanced MHC I antigen presentation to activate $CD8^+$ T cell antitumor immunity. Nano-ZSA51D combined with anti-PD-1 therapy achieved potent tumor remission in both colon and pancreatic cancer models. This study establishes Nano ZSA-51D as a novel strategy to reprogram HSPCs into antitumor neutrophils and highlights neutrophil programming as a potential approach for cancer immunotherapy.

MATERIALS AND METHODS

Cell cultures

All cells were maintained at 37 °C in a humidified atmosphere containing 5% CO2 and 95% air with 85% relative humidity. THP-1-Blue™ ISG cells (InvivoGen) were cultured in RPMI 1640 medium supplemented with 10% heat-inactivated fetal bovine serum (FBS; 30 min at 56 °C), 2 mM L-glutamine, 25 mM HEPES, 1 mM sodium pyruvate, 100 μg/ml normocin and 1% penicillin-streptomycin (Pen/Strep). LSK cells isolated from WT C57BL/6J mice were cultured in StemSpan medium (Stem Cell) supplemented with 50 ng ml^{-1} mouse SCF (Biolegend). Bone marrow neutrophils isolated from WT C57BL/6J mice and STING deficient mice (C57BL/6J-Sting1gt/J) were cultured in RPMI-1640 medium supplemented with 10% FBS, 2 mM L-glutamine, 25 mM HEPES, 1 mM sodium pyruvate, 50 μM β-mercaptoethanol, 0.1 mM nonessential amino acids, and 1% Pen/Strep. $CD8^+$ T cells are isolated from the spleens of OT-I transgenic mice were cultured in RPMI-1640 with 10% FBS, 2 mM L-glutamine, 25 mM HEPES, 1 mM sodium pyruvate, 50 μM β-mercaptoethanol, 0.1 mM nonessential amino acids, and 1% Pen/Strep. MC-38 colon adenocarcinoma cells and KPCY mouse pancreatic cancer cell lines (KPC 6620 and KPC 6422) were obtained from Kerafast. MC-38 cells were cultured in DMEM supplemented with 10% FBS, 2mM glutamine, 0.1 mM nonessential amino acids, 1 mM sodium pyruvate, 10 mM HEPES, 50 ug/ml gentamycin sulfate and 1% pen-strep. KPC 6620 and KPC 6422 cells were cultured in DMEM supplemented with Glutamax, 10% FBS, 1 mM sodium pyruvate and 1% Pen/Strep. The key reagents or resources were displayed in **Table S1**.

Mice

All animal experiments were conducted in accordance with protocols approved by the University of Michigan Committee on Use and Care of Animals (UCUCA). Animals were housed under pathogen-free conditions in temperature- and humidity-controlled environments, with free access

to food and water, and maintained on a 12-hour light/dark cycle at the unit for laboratory animal medicine (ULAM), part of the University of Michigan medical school office of research. WT C57BL6/J mice were obtained from the Charles River Laboratory. STING deficient mice (C57BL/6J-Sting1gt/J) and OT-I transgenic mice expressing a T cell receptor specific for the Ovalbumin-derived peptide SIINFEKL presented by H-2K^b (C57BL/6-Tg(TcraTcrb)1100Mjb/J) were purchased from the Jackson Laboratory. Mice aged 6–8 weeks were used for experiments, unless otherwise specified.

Tumor model

Tumor xenograft implantation experiments were performed using 6-week-old male WT C57BL/6 mice. 1×10^6 MC38 cells (murine colon adenocarcinoma cells), KPC 6620 or KPC 6422 cells (murine pancreatic cells) in 100 μL FBS-free DMEM medium were injected subcutaneously into the right lower flank of the C57BL6/J mice. The mice were randomly assigned for treatments when the mean tumor volume reached 50-100 mm^3 among all treatment groups 6 days after inoculation. Tumor growth and survival were monitored every two or three days. Tumor volume was calculated using the formula: Tumor volume = Length × Width^2/2, where length and width represent the longest and shortest tumor dimensions, respectively.

Synthesis and characterization of dimeric STING agonist ZSA-51D

The dimeric STING agonist ZSA-51D were synthesized based on our previously reported monomeric STING agonist ZSA-51 (**Fig. S1**).(*33, 68*) Briefly, starting material **1** was suspended in Et_2O and cooled to 0°C. MeMgBr was added to the suspension dropwise. The resulting mixture was stirred overnight to give intermediate **2**. **2** was stirred with PCC in DCM overnight to afford intermediate **3**. The solution of **3**, DIPEA and methyl thioglycolate in DMA was stirred at room temperature for 40 min under nitrogen atmosphere, followed by the addition of *t*-BuOK. The resulting mixture was heated at 80°C for 14 h to afford intermediate **4**. **4** was stirred with HATU, DCM, DIPEA and methyl 3-aminopropionate hydrochloride or *tert*-butyl 3-aminopropionate hydrochloride for 2 h at room temperature to provide intermediate **5a** or **5b**. **5a** or **5b** was deprotected under hydrogen atmosphere with palladium catalyst in ethanol to give intermediate **6a** or **6b**. **6a** or **6b** was dissolved in DCM. Then, TBDMSCl, imidazole and DMAP were added. The solution was stirred at room temperature for 0.5 h to give intermediate **7a** or 7**b**. The mixture of **7a** or **7b**, NBS, AIBN and CCl_4 was heated at 80°C for 2 h to produce intermediate **8a** or **8b**. **8a**

or **8b** was suspended in CH_3CN and cooled to 0°C. Then, NMO was added. The mixture was stirred at room temperature overnight to give intermediate **9a** or **9b**. **9a** or **9b** was dissolved in DCM followed by the addition of PCC. The suspension was stirred at room temperature for 16 h to furnish intermediate **10a** or **10b**. TBAF (0.25 mL, 1 M in THF) was added into the solution of **10a** or **10b** in THF. The solution was stirred at room temperature for 0.5 h to afford intermediate **11a** or **11b**. The mixture of **11a** or **11b**, K_2CO_3, catalytic amount of NaI, CH_3CN and 1,3-dibromopropane was heated at 80°C for 3 h to produce intermediate **12a** or **12b**. **12a** or **12b** was mixed **11a** or **11b**, K_2CO_3, catalytic amount of NaI and CH_3CN, and heated at 80°C for 4 h to provide target compound ZSA-51D or intermediate **13b**. **13b** was dissolved in DCM followed by the addition of TFA. The solution was stirred at room temperature for 3 h to afford target compound ZSA-52D.

hSTING protein binding assay

The human STING WT binding kit (Revvity) was obtained from PerkinElmer. Assays were performed according to the manufacturer's instructions using white opaque 386-well microplates. Briefly, 5 μL of test compounds at varying concentrations were mixed with 5 μL human STING WT protein (6×His-tagged protein), followed by the addition of 10 μL of a premixed working solutions containing the STING WT ligand d2 reagent and 6×His Tb cryptate-conjugated antibody. The reaction mixtures were incubated at room temperature for 3 hours. Homogeneous Time-Resolved Fluorescence (HTRF) signals of the reaction mixtures were measured using a Synergy 2 microplate reader (BioTek).

THP1-Blue ISG cell assay

THP1-Blue ISG cells (InvivoGen) are a human monocytic cell line engineered to express a secret embryonic alkaline phosphatase (SEAP) reporter gene under the control of an interferon-stimulated response element (ISRE). This system enables the detection of interferon regulatory factor (IRF) activation as an indicator of innate immune signaling. This assay detects IRF activation by quantifying SEAP activity in the culture supernatant using QUANTI-Blue™ (InvivoGen), a SEAP detection reagent.

Briefly, 100 μL of various concentrations of the test compounds were incubated with 100 μL of THP1-Blue ISG cell suspension (1×10^6 cells/mL) for 24 hours at 37°C. After incubation, 20 μL of the cell culture supernatant was mixed with 180 μL of freshly prepared QUANTI-Blue solution

in a 96-well plate and incubated at 37°C for 2 hours. SEAP activity was then measured using a Synergy 2 microplate reader (Biotek) at an absorbance of 620 nm. All samples were tested in triplicate, and appropriate vehicle-treated controls were included in each assay.

Preparation and characterization of Albumin-STING nanocomplex (Nano ZSA-51D)

Nano ZSA-51D was prepared following a previously established protocol.(*35*) Briefly, 10 mg of ZSA-51D was dissolved in 1mL of chloroform and emulsified with 100 mg of mouse serum albumin (Innovative Research) dissolved in 20 mL of Milli-Q water using a rotor-stator homogenizer to generate a milky emulsion. The emulsion was then processed through 6 cycles at 20,000 psi using a high-pressure homogenizer (Nano DeBEE) at 4°C. After homogenization, the organic solvent was removed under reduced pressure using a rotary evaporator at 25°C. The resulting Nano ZSA-51D suspension was lyophilized and stored at −20°C until further use. The size distribution of Nano ZSA-51D particles was measured by dynamic light scattering (DLS) using the Zetasizer Nano-ZS system (Malvern Instruments, UK). The measurements were performed three times for each sample and all the experiments were performed in triplicate.

Western blot analysis of STING pathway activation

Bone marrow-derived macrophages (BMDMs) were generated from bone marrow cells isolated from C57BL/6 mice and cultured as previously described.(*35*) BMDMs were treated with vehicle, free and Nano ZSA-51D at concentrations of 10 or 100 nM for 4 hours. After treatment, cells were lysed in RIPA buffer supplemented with protease and phosphatase inhibitors, followed by sonication and centrifugation at 12,000 × g for 15 minutes at 4°C. Protein concentrations were determined using a BCA assay (Thermo Fisher Scientific). Equal amounts of protein were separated by SDS-PAGE and transferred to PVDF membranes. Membranes were blocked with 5% non-fat milk in TBST and incubated with primary antibodies against STING, phospho-STING (Ser365), IRF3, phospho-IRF3 (Ser396), NF-κB p65, and phospho-NF-κB p65 (Ser536) (Cell Signaling Technology), followed by HRP-conjugated secondary antibodies. Signals were detected using enhanced chemiluminescence (ECL) reagents (Bio-Rad) and imaged with a ChemiDoc MP Imaging System (Bio-Rad).

ELISA cytokine quantification

Cytokine secretions after STING pathway activation were quantified using enzyme-linked immunosorbent assay (ELISA) kits according to the manufacturer's protocols. BMDMs were treated with vehicles, free ZSA-51D, or Nano ZSA-51D at concentrations of 100 nM for 48 hours. Cell culture supernatants were collected to measure the concentrations of IFN-β, TNF-α and IL-6 using mouse-specific ELISA kits (R&D Systems). Absorbance was read at 450 nm using a Synergy 2 microplate reader (Biotek), and cytokine concentrations were calculated based on standard curves generated with recombinant proteins provided in each kit.

Treatment regimen for in vivo studies

For STING agonist treatment, mice were intravenously administered with free or Nano ZSA-51D (1 mg/kg), free diABZI (1 mg/kg), or an equal volume of vehicle (15 mg/kg mouse serum albumin), as specified in the respective experimental workflow. Free ZSA-51D or diABZI was sequentially dissolved in DMSO and PEG-400 (1/4, v/v) to prepare a stock solution at 0.4 mg/mL. This stock was then diluted with an equal volume of PBS to yield a final formulation containing 0.2 mg/mL of the agonist for injection. Nano ZSA-51D was directly resuspended in PBS at 0.2 mg/mL for injection. For combination therapy, 100 μg of α-PD1 antibodies (Bio X Cell) were administrated intraperitoneally alongside STING agonist treatment, following the corresponding experimental schedule. α-PD1 antibodies were diluted using the recommended in vivo dilution buffer (Bio X Cell).

For in vivo antitumor efficacy studies, vehicles, free or Nano ZSA-51D, or free diABZI with/without α-PD1 were administered to tumor-bearing mice every 3 days for a total of 5 doses. For in vivo HSPC and immune profiling studies, the vehicle, free or Nano ZSA-51D with/without α-PD1 were administered to tumor-bearing mice every 3 days for 3 doses.

Single-cell suspension preparation for flow cytometry

Single-cell suspensions were prepared from the peripheral blood, bone marrow and tumor tissues after the STING agonist treatments. Peripheral blood (200 μL) was collected from the ophthalmic veins using heparinized calibrated pipettes at designed time points. Following euthanasia, tumors, femurs and tibia from the hind limbs were harvested and immediately placed on ice. Bone marrow cells were isolated by flushing tibias and femurs with ice-cold PBS containing 1% FBS and 1 mM EDTA through a 70 μm cell strainer (Tisch Scientific) into a 50 mL conical tube, followed by

centrifugation at 350 × g for 5 minutes. Tumors (< 1 g) were finely minced with surgical scissors and enzymatically dissociated in 5 mL RPMI 1640 (Thermo Scientific) containing 0.01–0.1% Collagenase/Hyaluronidase (STEMCELL Technologies) and 0.15 mg/mL DNase I (STEMCELL Technologies) at 37°C with shaking (400 rpm) for 30 min. Digested tumor suspensions were filtered through a 70 mm cell strainer, washed with ice-cold PBS supplemented with 1% FBS and 1 mM EDTA, and centrifuged at 350 × g for 5 min. Single-cell suspensions from blood, bone marrow, and tumor tissues were subjected to RBC lysis using ACK lysis buffer (Tonbo Biosciences) for 5 min at 4°C. Cells were then washed with PBS supplemented with 1% FBS, centrifuged at 400 × g for 5 min, and resuspended at 1×10^7 cells/mL in PBS prior to antibody staining and flow cytometric analysis.

Analysis of HSPC composition

For analysis and sorting of HSPC populations, single-cell suspensions from bone marrow enriched for lineage-negative (Lin-) cells using a biotin-conjugated anti-mouse lineage antibody panel (BioLegend), followed by magnetic separation according to the manufacturer's instructions. The enriched Lin^- cells were subsequently stained with fluorophore-conjugated antibodies (**Table S1**) against surface markers for flow cytometric analysis of HSPC subsets (**Fig. S19**).

Flow cytometry analysis

Sing-cell suspensions were first incubated with Ghost Dye™ Violet 510 (Tonbo Biosciences) for 30 min at 4°C to exclude dead cells, followed by washing and centrifugation at 400 × g for 5 minutes. Cells were then incubated with anti-mouse CD16/32 antibody (TruStain FcX™ PLUS; Biolegend) in PBS containing 1% FBS for 10 min at 4°C to block Fc receptors. Subsequently, cells were stained with fluorochrome-conjugated antibodies (**Table S1**) for 20 min at 4°C. After staining, cells were washed and centrifuged at 400 × g for 5 min, fixed using Fixation Buffer (BioLegend), and analyzed on a Cytek Aurora spectral flow cytometer. Data was processed using FlowJo software (BD biosciences (**Fig. S20**).

Cell sorting by fluorescence-activated cell sorting (FACS)

Neutrophils and their subpopulations were isolated from bone marrow treated in vitro with vehicle or Nano ZSA-51D (100 nM) using an MA900 Multi-Application Cell Sorter (Sony Biotechnology) equipped with a 100 μm sorting chip at 4°C. The bone marrow neutrophils were stained with

CD11b, Ly6G, CD101 and CD14. The dead cells were excluded by DAPI (5 μg/ml). The sorting purity exceeded 95%. Neutrophils were sorted as $CD11b^+Ly\text{-}6G^+$ cells. Neutrophil subsets were further gated and sorted within the $CD11b^+Ly\text{-}6G^+$ population based on CD101 and CD14 expression, yielding three distinct populations: $CD101^-CD14^-$, $CD101^-CD14^+$ and $CD101^+CD14^+$ populations. The sorted bone marrow neutrophils and their subpopulations were subsequently used for in vitro experiments, adaptive transfer experiments or bulk mRNA expression analysis. LSK cells were sorted as $Lin^-Sca\text{-}1^+c\text{-}Kit^+$ cells from enriched bone marrow Lin^- cells of WT C57BL/6J mice.

LSK culture and treatment in vitro

The sorted LSK cells were resuspended in StemSpan medium (Stem Cell) supplemented with 50 ng ml^{-1} mouse SCF (Biolegend) and seeded into U-shaped 96-well plate at a density of 2×10^4 cells per well. 100 nM of Nano ZSA-51D or 10 ng ml^{-1} cytokines (TNF-α, IFN-β, IFN-γ and IL-6) were added and incubated for 3 days. Following treatment, cells were collected, washed, and resuspended in PBS for flow cytometry analysis.

Reprogramming of bone marrow neutrophils in vitro

Bone marrow neutrophils were derived from the femurs and tibia of WT C57BL6/J mice or C57BL/6J-Tmem173-/- mice (female, 6-8 weeks old). Briefly, following euthanasia, femurs and tibia were harvested, and the bone marrow cells were flushed using ice-cold PBS containing 1% FBS and 1 mM EDTA. After centrifugation, red blood cells were lysed. The remaining cells were washed and resuspended in complete RPMI 1640 containing 10% fetal bovine serum (FBS), 2 mM L-glutamine, 25 mM HEPES, 1 mM sodium pyruvate, 50 μM β-mercaptoethanol and 1% Pen/Strep. Cells were seeded into sterile 12-well plate at a density of 5×10^6 cells per well. Free or Nano ZSA-51D (100 nM) was added with fresh complete RPMI 1640 and incubated overnight. Vehicle control (30 μg/ml mouse serum albumin) was included in parallel. In addition, the sorted bone marrow neutrophils were treated with 10 ng ml^{-1} cytokines (TNF-α, IFN-β, IFN-γ, IL-6 and TGF-β) for overnight. Following treatment, cells were collected, washed, and resuspended in PBS for flow cytometry analysis (**Fig. S21**).

Adoptive transfer therapy of neutrophil subsets

The sorted neutrophil subsets cells from bone marrow following treatment with Nano ZSA-51D (100 nM), including $CD101^{-}CD14^{-}$, $CD101^{-}CD14^{+}$ and $CD101^{+}CD14^{+}$ populations (2×10^{6} cells/mice), were adoptively transferred intratumorally (I.T.) into established MC-38 tumors. Concurrently, mice were received intraperitoneal (I.P.) injections of α-PD1 antibody (100 μg per mouse) every 2 days, as indicated in the treatment schedule. Tumor growth survival was measured every 2–3 days using digital calipers, and tumor volume was calculated according to the formula: Tumor volume = Length × $Width^2/2$, where length and width represent the longest and shortest tumor dimensions, respectively.

Tumors rechallenge and T cell memory analysis

To assess long-term antitumor immunity, cured mice were rechallenged with tumor cells at 100- or 120-days post-treatment. Specifically, 100 μL of MC-38 or KPC 6642 tumor cell suspension (5×10^{6} cells/mL) were subcutaneously injected into the left lower flank of the cured mice. Age-matched naïve mice were included as controls and received the same tumor inoculation. Tumor growth was monitored every 2–3 days starting from day 6 post-rechallenge. Tumor volume was calculated and recorded. At 180 days after tumor rechallenge, mice were euthanized, and spleens, lymph nodes, and peripheral blood were collected to prepare single-cell suspensions. $CD4^{+}$ and $CD8^{+}$ T cell memory subsets were analyzed by flow cytometry (**Fig. S22**).

Bulk mRNA-seq analysis

Neutrophils and their subpopulations ($CD101^{-}CD14^{+}$ and $CD101^{+}CD14^{+}$) were sorted from bone marrow cells following Nano ZSA-51D (100 nM) or vehicle treatment. Total RNA was extracted using RNeasy Plus Mini Kit (QIAGEN, #74134) according to the manufacturer's protocol. Only samples with an RNA Integrity Number (RIN) ⩾ 8 were used for library preparation.

Polyadenylated mRNA was isolated from 250 ng of total RNA using the NEBNext Poly(A) mRNA Magnetic Isolation Module (NEB, E7490) and converted into cDNA libraries using the NEBNext UltraExpress RNA Library Prep Kit (NEB, E3330L) and NEBNext Multiplex Oligos for Illumina (Unique Dual Index) (NEB, E6440L). The libraries were pooled and sequenced on the Illumina NovaSeq X 10B platform (paired end 150 bp, Illumina, 20085594) following the manufacturer's recommendations.

Raw reads were processed by trimming adapters and low-quality bases using Cutadapt (v4.8). Read quality was assessed using FastQC (v0.11.8), and potential contamination from foreign species was screened using Fastq Screen (v0.15.3). High-quality reads were aligned to the GRCm38 mouse reference genome (ENSEMBL) using STAR (v2.7.8a) with parameters optimized according to ENCODE best practices for RNA-seq. Gene- and transcript-level abundance estimation was performed using RSEM (v1.3.3). Alignment and quantification metrics were aggregated and summarized using MultiQC (v1.20).

Differential gene expression analysis was performed using the Bioconductor package DESeq2 (v1.30.0) on normalized and filtered count data. Genes with an adjusted p-value < 0.05 and an absolute $\log_2$ fold-change ($|\log_2 FC|$) > 1 were considered significantly differentially expressed. Over-Representation Analysis (ORA) was performed for KEGG pathways to identify enriched biological functions among the DEGs. Gene Set Enrichment Analysis (GSEA) was performed using KEGG and Gene Ontology (GO) gene sets based on the gene ranked list.

OT-I peptide (SIINFEKL) presentation on neutrophils

Bone marrow neutrophils were derived from the femurs and tibia of WT C57BL6/J mice. Bone marrow cells were seeded into sterile 24-well plate at a density of 1×10^6 cells per well. Cells were treated with OT-I peptide (CSSSIINFEKL, 50 μg/mL) and/or Nano ZSA-51D (100 nM) in fresh complete RPMI 1640 and incubated overnight. Vehicle control treated with 30 μg/mL mouse serum albumin under identical conditions. Following treatment, cells were collected, washed, and resuspended in PBS for flow cytometry analysis. To assess antigen presentation, cells were stained with PE conjugated anti-mouse MHC I and APC conjugated anti-mouse H-2K^b/SIINFEKL complex antibody. The expression of MHC I and the presentation of the OT-I peptide on neutrophils and their subsets were subsequently analyzed by flow cytometry.

OT-I CD8+ T cell activation and proliferation assays in vitro

OT-I CD8$^+$ T cells were isolated from OT-I transgenic mice (Jackson Laboratory, Cat. #003831) using the EasySep^{TM} mouse CD8$^+$ T cell isolation kit (STEMCELL Technologies, Cat. #19853) following the manufacturer's instructions. For proliferation analysis, OT-I CD8$^+$ T cells were labeled with the CellTrace™ Violet Cell Proliferation Kit (Thermo Scientific, Cat. #C34571) according to the manufacturer's protocol, followed by extensive washing to remove unbound dye.

Bone marrow neutrophils and their subsets ($CD101^{-}CD14^{+}$ and $CD101^{+}CD14^{+}$) were sorted from bone marrow cells following treatment with ovalbumin EndoFit™ (OVA, 200 μg/mL) and/or Nano ZSA-51D (100 nM), or vehicle control. Subsequently, CFSE- labeled OT-I CD8+ T cells and pre-treated neutrophils were co-cultured with a ratio of 1:2 (T cells: neutrophils) for 48 hours. OT-I $CD8^{+}$ T cells cultured alone under the same conditions served as a control group.

Following co-culture, cells were observed and imaged under bright field by EVOS M5000 microscopy (Invitrogen). T cell activation was assessed by staining with antibodies of activation markers CD69, CD25, and CD137 (4-1BB), followed by flow cytometry analysis. T cell proliferation was quantified based on CFSE fluorescence dilution.

In vivo toxicity evaluation of Nano ZSA-51D

To evaluate the in vivo safety profile of Nano ZSA-51D, comprehensive toxicity studies were performed using WT C57BL6/J mice. Six-week-old mice were randomly divided into three groups (n = 3 per group) and administered with vehicle (15 mg/kg mouse serum albumin), free or Nano ZSA-51D (1 mg/kg) via intravenous injection every three days for a total of five doses. Blood samples were collected on day 0, day 3, and day 15 following the initial dose for complete blood cell count. On day 15, plasma samples were collected to test liver function markers. Meanwhile, major organs, including the heart, liver, spleen, lung, kidney and intestine, were harvested and fixed for histopathological examination. All hematological, biochemical, and histopathological analyses were performed by the Unit for Laboratory Animal Medicine (ULAM).

Statistical analysis

All statistical analyses were performed using GraphPad Prism (version 10.3.1) unless otherwise specified. Data are presented as mean ± standard deviation (SD) as indicated in figure legends. Comparisons between two groups were performed using an unpaired two-tailed Student's T-test. For comparisons involving more than two groups, one-way or two-way analysis of variance (ANOVA) followed by Tukey's or Sidak's multiple comparison test was used as appropriate. For survival analyses, Kaplan–Meier curves were plotted and compared using the log-rank (Mantel–Cox) test. A p-value < 0.05 was considered statistically significant. Specific statistical tests used for each experiment are detailed in the figure legends.

List of Supplementary Materials

Fig. S1 to S22

Table S1

Reference:

1. S. R. Woo, M. B. Fuertes, L. Corrales, S. Spranger, M. J. Furdyna, M. Y. K. Leung, R. Duggan, Y. Wang, G. N. Barber, K. A. Fitzgerald, M. L. Alegre, T. F. Gajewski, STING-Dependent Cytosolic DNA Sensing Mediates Innate Immune Recognition of Immunogenic Tumors. *Immunity* **41**, 830-842 (2014).
2. B. Jneid, A. Bochnakian, C. Hoffmann, F. Delisle, E. Djacoto, P. Sirven, J. Denizeau, C. Sedlik, Y. Gerber-Ferder, F. Fiore, R. Akyol, C. Brousse, R. Kramer, I. Walters, S. Carlioz, H. Salmon, B. Malissen, M. Dalod, E. Piaggio, N. Manel, Selective STING stimulation in dendritic cells primes antitumor T cell responses. *Sci Immunol* **8**, eabn6612 (2023).
3. J. Wang, S. Li, M. Wang, X. Wang, S. Chen, Z. Sun, X. Ren, G. Huang, B. D. Sumer, N. Yan, Y. X. Fu, J. Gao, STING licensing of type I dendritic cells potentiates antitumor immunity. *Sci Immunol* **9**, eadj3945 (2024).
4. Q. Wang, J. S. Bergholz, L. Ding, Z. Lin, S. K. Kabraji, M. E. Hughes, X. He, S. Xie, T. Jiang, W. Wang, J. J. Zoeller, H. J. Kim, T. M. Roberts, P. A. Konstantinopoulos, U. A. Matulonis, D. A. Dillon, E. P. Winer, N. U. Lin, J. J. Zhao, STING agonism reprograms tumor-associated macrophages and overcomes resistance to PARP inhibition in BRCA1-deficient models of breast cancer. *Nat Commun* **13**, 3022 (2022).
5. H. Ishikawa, G. N. Barber, STING is an endoplasmic reticulum adaptor that facilitates innate immune signalling. *Nature* **455**, 674-U674 (2008).
6. K. R. Balka, C. Louis, T. L. Saunders, A. M. Smith, D. J. Calleja, D. B. D'Silva, F. Moghaddas, M. Tailler, K. E. Lawlor, Y. F. Zhan, C. J. Burns, I. P. Wicks, J. J. Miner, B. T. Kile, S. L. Masters, D. De Nardo, TBK1 and IKKε Act Redundantly to Mediate STING-Induced NF-κB Responses in Myeloid Cells. *Cell Rep* **31**, (2020).
7. B. R. Kimmel, K. Arora, N. C. Chada, V. Bharti, A. J. Kwiatkowski, J. E. Finkelstein, A. Hanna, E. N. Arner, T. L. Sheehy, L. E. Pastora, J. M. Yang, H. M. Pagendarm, P. T. Stone, E. Hargrove-Wiley, B. C. Taylor, L. A. Hubert, B. M. Fingleton, K. N. Gibson-Corley, J. C. May, J. A. McLean, J. C. Rathmell, A. Richmond, W. K. Rathmell, J. M. Balko, J. T. Wilson, Potentiating cancer immunotherapies with modular albumin-hitchhiking nanobody-STING agonist conjugates. *Nat Biomed Eng*, (2025).
8. S. Ye, J. Gao, Hitchhiking albumin to STING tumours. *Nat Biomed Eng*, (2025).
9. M. Nagata, A. Kosaka, Y. Yajima, S. Yasuda, M. Ohara, K. Ohara, S. Harabuchi, R. Hayashi, H. Funakoshi, J. Ueda, T. Kumai, T. Nagato, K. Oikawa, Y. Harabuchi, C. Esteban, T. Ohkuri, H. Kobayashi, A critical role of STING-triggered tumor-migrating neutrophils for anti-tumor effect of intratumoral cGAMP treatment. *Cancer Immunol Immun* **70**, 2301-2312 (2021).
10. T. X. Xu, J. Dai, L. R. Tang, L. Z. Sun, L. Si, J. Guo, Systemic administration of STING agonist promotes myeloid cells maturation and antitumor immunity through

regulating hematopoietic stem and progenitor cell fate. *Cancer Immunol Immun*, (2023).

11. M. Munder, H. Schneider, C. Luckner, T. Giese, C. D. Langhans, J. M. Fuentes, P. Kropf, I. Mueller, A. Kolb, M. Modolell, A. D. Ho, Suppression of T-cell functions by human granulocyte arginase. *Blood* **108**, 1627-1634 (2006).
12. H. Zhang, X. Zhu, T. J. Friesen, J. W. Kwak, T. Pisarenko, S. Mekvanich, M. A. Velasco, T. W. Randolph, J. Kargl, A. M. Houghton, Annexin A2/TLR2/MYD88 pathway induces arginase 1 expression in tumor-associated neutrophils. *J Clin Invest* **132**, (2022).
13. A. J. Templeton, M. G. McNamara, B. Seruga, F. E. Vera-Badillo, P. Aneja, A. Ocana, R. Leibowitz-Amit, G. Sonpavde, J. J. Knox, B. Tran, I. F. Tannock, E. Amir, Prognostic role of neutrophil-to-lymphocyte ratio in solid tumors: a systematic review and meta-analysis. *J Natl Cancer Inst* **106**, dju124 (2014).
14. H. Raskov, A. Orhan, S. Gaggar, I. Gögenur, Neutrophils and polymorphonuclear myeloid-derived suppressor cells: an emerging battleground in cancer therapy. *Oncogenesis* **11**, (2022).
15. J. L. Su, Y. N. Li, S. H. Tan, T. L. Cheng, Y. Z. Luo, L. M. Zhang, Pretreatment neutrophil-to-lymphocyte ratio is associated with immunotherapy efficacy in patients with advanced cancer: a systematic review and meta-analysis. *Sci Rep-Uk* **15**, (2025).
16. K. G. Mitchell, L. X. Diao, T. Karpinets, M. V. Negrao, H. T. Tran, E. R. Parra, E. M. Corsini, A. Reuben, L. Federico, C. Bernatchez, H. Dejima, A. Francisco-Cruz, J. Wang, M. B. Antonoff, A. A. Vaporciyan, S. G. Swisher, T. Cascone, I. I. Wistuba, J. V. Heymach, D. L. Gibbons, J. J. Zhang, C. L. Haymaker, B. Sepesi, Neutrophil expansion defines an immunoinhibitory peripheral and intratumoral inflammatory milieu in resected non-small cell lung cancer: a descriptive analysis of a prospectively immunoprofiled cohort. *J Immunother Cancer* **8**, (2020).
17. X. Huang, E. Nepovimova, V. Adam, L. Sivak, Z. Heger, M. Valko, Q. Wu, K. Kuca, Neutrophils in Cancer immunotherapy: friends or foes? *Mol Cancer* **23**, 107 (2024).
18. M. Zhang, H. Qin, Y. Wu, Q. Gao, Complex role of neutrophils in the tumor microenvironment: an avenue for novel immunotherapies. *Cancer Biol Med* **21**, 849-863 (2024).
19. E. Eruslanov, Y. Nefedova, D. I. Gabrilovich, The heterogeneity of neutrophils in cancer and its implication for therapeutic targeting. *Nat Immunol* **26**, 17-28 (2025).
20. M. Siwicki, M. J. Pittet, Versatile neutrophil functions in cancer. *Semin Immunol* **57**, 101538 (2021).
21. I. L. Linde, T. R. Prestwood, J. T. Qiu, G. Pilarowski, M. H. Linde, X. Y. Zhang, L. Shen, N. E. Reticker-Flynn, D. K. C. Chiu, L. Y. Sheu, S. Van Deursen, L. L. Tolentino, W. C. Song, E. G. Engleman, Neutrophil-activating therapy for the treatment of cancer. *Cancer Cell* **41**, 356-+ (2023).
22. D. Hirschhorn, S. Budhu, L. Kraehenbuehl, M. Gigoux, D. Schröder, A. Chow, J. M. Ricca, B. Gasmi, O. De Henau, L. M. B. Mangarin, Y. Y. Li, L. Hamadene, A. L. Flamar, H. Choi, C. A. Cortez, C. L. Liu, A. Holland, S. Schad, I. Schulze, A. B. Warner, T. J. Hollmann, A. Arora, K. S. Panageas, G. A. Rizzuto, R. Duhen, A. D. Weinberg, C. N. Spencer, D. Ng, X. Y. He, J. Albrengues, D. Redmond, M. Egeblad, J. D. Wolchok, T.

Merghoub, T cell immunotherapies engage neutrophils to eliminate tumor antigen escape variants. *Cell* **186**, 1432-+ (2023).

23. A. Ager, Cancer immunotherapy: T cells and neutrophils working together to attack cancers. *Cell* **186**, 1304-1306 (2023).

24. N. Kumbhojkar, S. Prakash, T. Fukuta, K. Adu-Berchie, N. Kapate, R. C. Y. An, S. Darko, V. C. Suja, K. S. Park, A. P. Gottlieb, M. G. Bibbey, M. Mukherji, L. L. W. Wang, D. J. Mooney, S. Mitragotri, Neutrophils bearing adhesive polymer micropatches as a drug-free cancer immunotherapy. *Nat Biomed Eng* **8**, (2024).

25. M. Benguigui, T. J. Cooper, P. Kalkar, S. Schif-Zuck, R. Halaban, A. Bacchiocchi, I. Kamer, A. Deo, B. Manobla, R. Menachem, J. Haj-Shomaly, A. Vorontsova, Z. Raviv, C. Buxbaum, P. Christopoulos, J. Bar, M. Lotem, M. Sznol, A. Ariel, S. S. Shen-Orr, Y. Shaked, Interferon-stimulated neutrophils as a predictor of immunotherapy response. *Cancer Cell* **42**, (2024).

26. Y. Wu, J. Ma, X. Yang, F. Nan, T. Zhang, S. Ji, D. Rao, H. Feng, K. Gao, X. Gu, S. Jiang, G. Song, J. Pan, M. Zhang, Y. Xu, S. Zhang, Y. Fan, X. Wang, J. Zhou, L. Yang, J. Fan, X. Zhang, Q. Gao, Neutrophil profiling illuminates anti-tumor antigen-presenting potency. *Cell* **187**, 1422-1439 e1424 (2024).

27. V. Mysore, X. Cullere, J. Mears, F. Rosetti, K. Okubo, P. X. Liew, F. Zhang, I. Madera-Salcedo, F. Rosenbauer, R. M. Stone, J. C. Aster, U. H. von Andrian, A. H. Lichtman, S. Raychaudhuri, T. N. Mayadas, FcγR engagement reprograms neutrophils into antigen cross-presenting cells that elicit acquired anti-tumor immunity. *Nature Communications* **12**, (2021).

28. H. Garner, M. Martinovic, N. Q. Liu, N. A. M. Bakker, I. Q. Velilla, C. S. Hau, K. Vrijland, D. Kaldenbach, M. Kok, E. de Wit, K. E. de Visser, Understanding and reversing mammary tumor-driven reprogramming of myelopoiesis to reduce metastatic spread. *Cancer Cell*, (2025).

29. L. Dong, L. G. Ng, Tumor neutrophils rewired from birth. *Cancer Cell*, (2025).

30. A. W. Daman, A. C. Antonelli, G. Redelman-Sidi, L. Paddock, S. Khayat, M. Ketavarapu, J. G. Cheong, L. F. Jurado, A. Benjamin, S. Jiang, D. Ahimovic, V. R. Lawless, M. J. Bale, O. Loutochin, V. A. McPherson, M. Divangahi, R. E. Niec, D. Pe'er, E. Pietzak, S. Z. Josefowicz, M. S. Glickman, Microbial cancer immunotherapy reprograms hematopoiesis to enhance myeloid-driven anti-tumor immunity. *Cancer Cell*, (2025).

31. J. Qian, C. Ma, Q. T. Waterbury, X. Zhi, C. S. Moon, R. Tu, H. Kobayashi, F. Wu, B. Zheng, Y. Zeng, H. Zheng, Y. Ochiai, R. A. White, D. W. Harle, J. S. LaBella, L. B. Zamechek, L. ZhongMing Hu, R. H. Moy, A. S. Han, B. L. Daugherty, S. Lederman, T. C. Wang, A CXCR4 partial agonist improves immunotherapy by targeting immunosuppressive neutrophils and cancer-driven granulopoiesis. *Cancer Cell* **43**, 1512-1529 e1511 (2025).

32. J. Gungabeesoon, N. A. Gort-Freitas, M. Kiss, E. Bolli, M. Messemaker, M. Siwicki, M. Hicham, R. Bill, P. Koch, C. Cianciaruso, F. Duval, C. Pfirschke, M. Mazzola, S. Peters, K. Homicsko, C. Garris, R. Weissleder, A. M. Klein, M. J. Pittet, A neutrophil response linked to tumor control in immunotherapy. *Cell* **186**, 1448-1464 e1420 (2023).

33. H. Y. Zhao, Z. W. Liu, J. S. Tao, S. Mao, M. L. Wang, M. He, B. Wen, W. Gao, D. X. Sun, An oral tricyclic STING agonist suppresses tumor growth through remodeling of the immune microenvironment. *Cell Chem Biol* **32**, (2025).
34. E. N. Hoogenboezem, C. L. Duvall, Harnessing albumin as a carrier for cancer therapies. *Adv Drug Deliver Rev* **130**, 73-89 (2018).
35. Y. D. Song, L. Bugada, R. T. Li, H. X. Hu, L. C. Zhang, C. Y. Li, H. B. Yuan, K. K. Rajanayake, N. A. Truchan, F. Wen, W. Gao, D. X. Sun, Albumin nanoparticle containing a PI3Kγ inhibitor and paclitaxel in combination with α-PD1 induces tumor remission of breast cancer in mice. *Sci Transl Med* **14**, (2022).
36. D. Sun, S. Zhou, W. Gao, What Went Wrong with Anticancer Nanomedicine Design and How to Make It Right. *ACS Nano* **14**, 12281-12290 (2020).
37. E. M. Pietras, D. Reynaud, Y. A. Kang, D. Carlin, F. J. Calero-Nieto, A. D. Leavitt, J. M. Stuart, B. Göttgens, E. Passegué, Functionally Distinct Subsets of Lineage-Biased Multipotent Progenitors Control Blood Production in Normal and Regenerative Conditions. *Cell Stem Cell* **17**, 35-46 (2015).
38. S. Singhal, P. S. Bhojnagarwala, S. O'Brien, E. K. Moon, A. L. Garfall, A. S. Rao, J. G. Quatromoni, T. L. Stephen, L. Litzky, C. Deshpande, M. D. Feldman, W. W. Hancock, J. R. Conejo-Garcia, S. M. Albelda, E. B. Eruslanov, Origin and Role of a Subset of Tumor-Associated Neutrophils with Antigen-Presenting Cell Features in Early-Stage Human Lung Cancer. *Cancer Cell* **30**, 120-135 (2016).
39. S. Saha, S. K. Biswas, Tumor-Associated Neutrophils Show Phenotypic and Functional Divergence in Human Lung Cancer. *Cancer Cell* **30**, 11-13 (2016).
40. C. Y. Liu, Y. M. Wang, C. L. Wang, P. H. Feng, H. W. Ko, Y. H. Liu, Y. C. Wu, Y. Chu, F. T. Chung, C. H. Kuo, K. Y. Lee, S. M. Lin, H. C. Lin, C. H. Wang, C. T. Yu, H. P. Kuo, Population alterations of L-arginase- and inducible nitric oxide synthase-expressed CD11b+/CD14(-)/CD15+/CD33+ myeloid-derived suppressor cells and CD8+ T lymphocytes in patients with advanced-stage non-small cell lung cancer. *J Cancer Res Clin Oncol* **136**, 35-45 (2010).
41. M. Evrard, I. W. H. Kwok, S. Z. Chong, K. W. W. Teng, E. Becht, J. Chen, J. L. Sieow, H. L. Penny, G. C. Ching, S. Devi, J. M. Adrover, J. L. Y. Li, K. H. Liong, L. Tan, Z. Poon, S. Foo, J. W. Chua, I. H. Su, K. Balabanian, F. Bachelerie, S. K. Biswas, A. Larbi, W. Y. K. Hwang, V. Madan, H. P. Koeffler, S. C. Wong, E. W. Newell, A. Hidalgo, F. Ginhoux, L. G. Ng, Developmental Analysis of Bone Marrow Neutrophils Reveals Populations Specialized in Expansion, Trafficking, and Effector Functions. *Immunity* **48**, 364-379 e368 (2018).
42. H. I. Muendlein, W. M. Connolly, J. Cameron, D. Jetton, Z. Magri, I. Smirnova, E. Vannier, X. D. Li, A. J. Martinot, R. Batorsky, A. Poltorak, Neutrophils and macrophages drive TNF-induced lethality via TRIF/CD14-mediated responses. *Science Immunology* **7**, (2022).
43. N. S. Hackert, F. A. Radtke, T. Exner, H. M. Lorenz, C. Mueller-Tidow, P. A. Nigrovic, G. Wabnitz, R. Grieshaber-Bouyer, Human and mouse neutrophils share core transcriptional programs in both homeostatic and inflamed contexts. *Nature Communications* **14**, (2023).

44. D. Sharygin, L. G. Koniaris, C. Wells, T. A. Zimmers, T. Hamidi, Role of CD14 in human disease. *Immunology* **169**, 260-270 (2023).
45. J. Pugin, D. Heumann, A. Tomasz, V. V. Kravchenko, Y. Akamatsu, M. Nishijima, M. P. Glauser, P. S. Tobias, R. J. Ulevitch, Cd14 Is a Pattern-Recognition Receptor. *Immunity* **1**, 509-516 (1994).
46. Z. M. Ding, J. E. Babensee, S. I. Simon, H. F. Lu, J. L. Perrard, D. C. Bullard, X. Y. Dai, S. K. Bromley, M. L. Dustin, M. L. Entman, C. W. Smith, C. M. Ballantyne, Relative contribution of LFA-1 and Mac-1 to neutrophil adhesion and migration. *J Immunol* **163**, 5029-5038 (1999).
47. T. M. Carlos, J. M. Harlan, Leukocyte-Endothelial Adhesion Molecules. *Blood* **84**, 2068-2101 (1994).
48. J. Y. Li, K. T. Byme, F. X. Yan, T. Yamazoe, Z. Y. Chen, T. Baslan, L. P. Richman, J. H. Lin, Y. H. Sun, A. J. Rech, D. Balli, C. A. Hay, Y. Sela, A. J. Merrell, S. M. Liudahl, N. Gordon, R. J. Norgard, S. Yuan, S. X. Yu, T. Chao, S. Ye, T. S. K. Eisinger-Mathason, R. B. Faryabi, J. W. Tobias, S. W. Lowe, L. M. Coussens, E. J. Wherry, R. H. Vonderheide, B. Z. Stangert, Tumor Cell-Intrinsic Factors Underlie Heterogeneity of Immune Cell Infiltration and Response to Immunotherapy. *Immunity* **49**, 178-+ (2018).
49. Z. G. Fridlender, J. Sun, S. Kim, V. Kapoor, G. J. Cheng, L. N. Ling, G. S. Worthen, S. M. Albelda, Polarization of Tumor-Associated Neutrophil Phenotype by TGF-β: "N1" versus "N2" TAN. *Cancer Cell* **16**, 183-194 (2009).
50. H. Piccard, R. J. Muschel, G. Opdenakker, On the dual roles and polarized phenotypes of neutrophils in tumor development and progression. *Crit Rev Oncol Hematol* **82**, 296-309 (2012).
51. J. Zhang, J. Gu, X. Wang, C. Ji, D. Yu, M. Wang, J. Pan, H. A. Santos, H. Zhang, X. Zhang, Engineering and Targeting Neutrophils for Cancer Therapy. *Adv Mater* **36**, e2310318 (2024).
52. W. M. Schneider, M. D. Chevillotte, C. M. Rice, Interferon-stimulated genes: a complex web of host defenses. *Annu Rev Immunol* **32**, 513-545 (2014).
53. E. Duong, T. B. Fessenden, E. Lutz, T. Dinter, L. Yim, S. Blatt, A. Bhutkar, K. D. Wittrup, S. Spranger, Type I interferon activates MHC class I-dressed CD11b(+) conventional dendritic cells to promote protective anti-tumor CD8(+) T cell immunity. *Immunity* **55**, 308-323 e309 (2022).
54. T. Kawai, S. Akira, Toll-like Receptors and Their Crosstalk with Other Innate Receptors in Infection and Immunity. *Immunity* **34**, 637-650 (2011).
55. T. Kawai, S. Akira, The roles of TLRs, RLRs and NLRs in pathogen recognition. *Int Immunol* **21**, 317-337 (2009).
56. K. Wicherska-Pawlowska, T. Wrobel, J. Rybka, Toll-Like Receptors (TLRs), NOD-Like Receptors (NLRs), and RIG-I-Like Receptors (RLRs) in Innate Immunity. TLRs, NLRs, and RLRs Ligands as Immunotherapeutic Agents for Hematopoietic Diseases. *Int J Mol Sci* **22**, (2021).
57. H. M. Yan, T. Kamiya, P. Suabjakyong, N. M. Tsuji, Targeting C-type lectin receptors for cancer immunity. *Front Immunol* **6**, (2015).
58. D. Reynaud, E. Pietras, K. Barry-Holson, A. Mir, M. Binnewies, M. Jeanne, O. Sala-Torra, J. P. Radich, E. Passegué, IL-6 Controls Leukemic Multipotent Progenitor Cell Fate and

Contributes to Chronic Myelogenous Leukemia Development. *Cancer Cell* **20**, 661-673 (2011).

59. I. Zanoni, Y. H. Tan, M. Di Gioia, J. R. Springstead, J. C. Kagan, By Capturing Inflammatory Lipids Released from Dying Cells, the Receptor CD14 Induces Inflammasome-Dependent Phagocyte Hyperactivation. *Immunity* **47**, 697-+ (2017).
60. N. W. J. Schröder, S. Morath, C. Alexander, L. Hamann, T. Hartung, U. Zähringer, U. B. Göbel, J. R. Weber, R. R. Schumann, Lipoteichoic acid (LTA) of and activates immune cells via toll-like receptor (TLR)-2, lipopolysaccharide-binding protein (LBP), and CD14, whereas TLR-4 and MD-2 are not involved. *J Biol Chem* **278**, 15587-15594 (2003).
61. H. Roedig, M. V. Nastase, H. Frey, K. Moreth, J. Zeng-Brouwers, C. Poluzzi, L. T. H. Hsieh, C. Brandts, S. Fulda, M. Wygrecka, L. Schaefer, Biglycan is a new high-affinity ligand for CD14 in macrophages. *Matrix Biol* **77**, 4-22 (2019).
62. A. Woodfin, M. Beyrau, M. B. Voisin, B. Ma, J. R. Whiteford, P. L. Hordijk, N. Hogg, S. Nourshargh, ICAM-1-expressing neutrophils exhibit enhanced effector functions in murine models of endotoxemia. *Blood* **127**, 898-907 (2016).
63. J. B. Hines, A. J. Kacew, R. F. Sweis, The Development of STING Agonists and Emerging Results as a Cancer Immunotherapy. *Curr Oncol Rep* **25**, 189-199 (2023).
64. L. Motedayen Aval, J. E. Pease, R. Sharma, D. J. Pinato, Challenges and Opportunities in the Clinical Development of STING Agonists for Cancer Immunotherapy. *J Clin Med* **9**, (2020).
65. B. Wang, W. Yu, H. Jiang, X. Meng, D. Tang, D. Liu, Clinical applications of STING agonists in cancer immunotherapy: current progress and future prospects. *Front Immunol* **15**, 1485546 (2024).
66. J. M. Ramanjulu, G. S. Pesiridis, J. Yang, N. Concha, R. Singhaus, S. Y. Zhang, J. L. Tran, P. Moore, S. Lehmann, H. C. Eberl, M. Muelbaier, J. L. Schneck, J. Clemens, M. Adam, J. Mehlmann, J. Romano, A. Morales, J. Kang, L. Leister, T. L. Graybill, A. K. Charnley, G. Ye, N. Nevins, K. Behnia, A. I. Wolf, V. Kasparcova, K. Nurse, L. Wang, A. C. Puhl, Y. Li, M. Klein, C. B. Hopson, J. Guss, M. Bantscheff, G. Bergamini, M. A. Reilly, Y. Lian, K. J. Duffy, J. Adams, K. P. Foley, P. J. Gough, R. W. Marquis, J. Smothers, A. Hoos, J. Bertin, Design of amidobenzimidazole STING receptor agonists with systemic activity. *Nature* **564**, 439-443 (2018).
67. E. N. Chin, C. Yu, V. F. Vartabedian, Y. Jia, M. Kumar, A. M. Gamo, W. Vernier, S. H. Ali, M. Kissai, D. C. Lazar, N. Nguyen, L. E. Pereira, B. Benish, A. K. Woods, S. B. Joseph, A. Chu, K. A. Johnson, P. N. Sander, F. Martinez-Pena, E. N. Hampton, T. S. Young, D. W. Wolan, A. K. Chatterjee, P. G. Schultz, H. M. Petrassi, J. R. Teijaro, L. L. Lairson, Antitumor activity of a systemic STING-activating non-nucleotide cGAMP mimetic. *Science* **369**, 993-999 (2020).
68. B. S. Pan, S. A. Perera, J. A. Piesvaux, J. P. Presland, G. K. Schroeder, J. N. Cumming, B. W. Trotter, M. D. Altman, A. V. Buevich, B. Cash, S. Cemerski, W. Chang, Y. P. Chen, P. J. Dandliker, G. Feng, A. Haidle, T. Henderson, J. Jewell, I. Kariv, I. Knemeyer, J. Kopinja, B. M. Lacey, J. Laskey, C. A. Lesburg, R. Liang, B. J. Long, M. Lu, Y. H. Ma, E. C. Minnihan, G. O'Donnell, R. Otte, L. Price, L. Rakhilina, B. Sauvagnat, S. Sharma, S.

Tyagarajan, H. Woo, D. F. Wyss, S. Xu, D. J. Bennett, G. H. Addona, An orally available non-nucleotide STING agonist with antitumor activity. *Science* **369**, 935-+ (2020).
69. H. Y. Zhao, J. S. Tao, L. C. Zhang, Q. X. Li, M. He, B. Wen, Z. W. Liu, H. Myatt, D. X. Sun, Design of an Oral STING Agonist through Intramolecular Hydrogen Bond Ring Mimicking to Achieve Complete Tumor Regression. *J Med Chem* **68**, 11365-11385 (2025).

Acknowledgements

We thank the University of Michigan Unit for Laboratory Animal Medicine (ULAM) for support in maintaining laboratory animals, and the In Vivo Animal Core (IVAC) for assistance toxicity studies. We also acknowledge the University of Michigan Pharmacokinetics Core, Flow Cytometry Core, Genomics Core for technical service.

Author contributions

J.T., W.G., and D.S. conceived the project, developed the hypotheses, designed the experiments and wrote the manuscript; J.T. performed most experiments and analyzed data, with assistance from all authors; H.Z. conducted the chemical synthesis. C.L. provided support for bioinformatic analysis. H.W. and F.K. assisted with the in vivo flow cytometry studies. Q.L., M.H. and B.W. assisted with the in vivo pharmacokinetic studies. Z.L. tested the STING binding and cellular activity in vitro. D.S. supervised the project and acquired funding.

Competing interests

University of Michigan has filed a patent based on these studies where some authors are listed as inventors.

Data and materials availability

All data associated with this study are present in the paper or the Supplementary Materials. Materials can be made available through a material transfer agreement with D.S.